



**Measurement of Exclusive B Lifetimes in the modes
 $B^+ \rightarrow J/\psi K^+$, $B^0 \rightarrow J/\psi K^{*0}$, $B^0 \rightarrow J/\psi K_s^0$, $B_s^0 \rightarrow J/\psi \phi$ and $\Lambda_b \rightarrow J/\psi \Lambda$, and
measurement of the B^+/B^0 , B_s^0/B^0 and Λ_b/B^0 lifetime ratios.**

Text for the blessed web page – CDF note 8524

The CDF Collaboration
URL <http://www-cdf.fnal.gov>
(Dated: December 21, 2006)

We present an updated measurement of exclusive B lifetimes in the modes $B^+ \rightarrow J/\psi K^+$, $B^0 \rightarrow J/\psi K^{*0}$, $B^0 \rightarrow J/\psi K_s^0$, $B_s^0 \rightarrow J/\psi \phi$ and $\Lambda_b \rightarrow J/\psi \Lambda$, based upon 1.0 fb^{-1} of luminosity collected between February 2002 and March 2006. We measure:

$$\begin{aligned}c\tau(B^+) &= 488.6 \pm 4.8(\text{stat.}) \pm 3.2(\text{syst.})\mu\text{m} \\c\tau(B^0) &= 465.1 \pm 5.8(\text{stat.}) \pm 3.2(\text{syst.})\mu\text{m} \\c\tau(B_s^0) &= 447.9 \pm 16.2(\text{stat.}) \pm 2.8(\text{syst.})\mu\text{m} \\c\tau(\Lambda_b) &= 473.8 \pm 23.1(\text{stat.}) \pm 3.5(\text{syst.})\mu\text{m}\end{aligned}$$

This corresponds to

$$\begin{aligned}\tau(B^+) &= 1.630 \pm 0.016 (\text{stat.}) \pm 0.011 (\text{syst.})\text{ps} \\ \tau(B^0) &= 1.551 \pm 0.019 (\text{stat.}) \pm 0.011 (\text{syst.})\text{ps} \\ \tau(B_s^0) &= 1.494 \pm 0.054 (\text{stat.}) \pm 0.009 (\text{syst.})\text{ps} \\ \tau(\Lambda_b) &= 1.580 \pm 0.077 (\text{stat.}) \pm 0.012 (\text{syst.})\text{ps}\end{aligned}$$

We also present a measurement of the lifetime ratios

$$\begin{aligned}\tau(B^+)/\tau(B^0) &= 1.051 \pm 0.023 (\text{stat.}) \pm 0.004 (\text{syst.}), \\ \tau(B_s^0 \rightarrow J/\psi \phi)/\tau(B^0) &= 0.963 \pm 0.047 (\text{stat.}) \pm 0.005 (\text{syst.}) \\ \tau(\Lambda_b)/\tau(B^0) &= 1.018 \pm 0.062 (\text{stat.}) \pm 0.007 (\text{syst.})\end{aligned}$$

I. INTRODUCTION

A. Theoretical context

The measured lifetimes of hadrons with a heavy quark will allow us to test the accuracy of a theoretical approach to the study of heavy flavor physics known as the Heavy Quark Expansion [1]. This is a type of operator product expansion of observable quantities such as inclusive decay rates, which separates long- and short-distance scale physics, and whose terms are proportional to powers of Λ_{QCD}/m_b . The expansion:

$$\Gamma = \frac{G_F^2 m_b^5}{192\pi^3} |V_{cb}|^2 \cdot \left[A_0 + A_2 \left(\frac{\Lambda_{QCD}}{m_b} \right)^2 + A_3 \left(\frac{\Lambda_{QCD}}{m_b} \right)^3 \right] \quad (1)$$

is rapidly convergent and leads to precise predictions in the case of bottom hadrons. The heavy quark expansion predicts b-hadron lifetime differences of only up to about ten percent, much smaller than in the charm system where the charged and neutral D meson lifetimes differ by more than a factor of two. The trend towards lower lifetime differences with heavier quark masses is easily seen to be a feature of expansion (1) and is a reflection of the fact that the energies released in the decay of a bottom quark are much higher than the energy of interaction with the light quark cloud surrounding the heavy, to first approximation stationary, bottom quark.

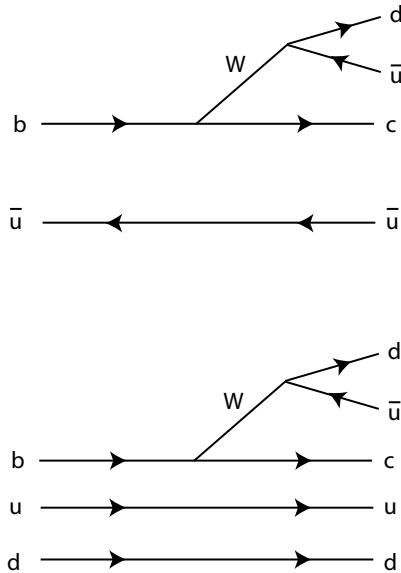


FIG. 1: Spectator diagrams in b-hadron decay. Top: b meson decay. Bottom: b baryon decay.

At lowest order in Λ_{QCD}/m_b the heavy quark is a static source of color field which decays as in the spectator model, with no interaction with the light quark cloud and the same lifetime for all species of b-hadron. The first order at which splitting of lifetimes between different species occurs is $(\Lambda_{QCD}/m_b)^2$, where Fermi motion of the b-quark and interactions between its spin and that of the light quark cloud enter. Differences between mesons and baryons appear at this order: the baryons, surrounded by two light quarks in a spin 0 cloud, decay more easily (faster) than the mesons surrounded by a spin 1/2 antiquark cloud. This decreases the baryon lifetime by about 2% relative to that of the mesons. At order $(\Lambda_{QCD}/m_b)^3$, spectator effects appear, enhanced by a favorable phase space factor. These are Pauli Interference and Weak Annihilation (mesons) or Weak Scattering (baryons); and occur through classes of diagrams with short-distance interactions typified by Fig. 2, and Fig. 3. For b baryons the third order contributions are larger than those of second order because of more-or-less accidental cancellations and the phase space factor. Pauli interference significantly prolongs the lifetime of the B^+ relative to the B^0 , while weak annihilation is a smaller effect. The predictions for B hadron lifetimes is shown in Table I. [11] The principal assumption of the HQE is that of quark-hadron duality, which holds that the detailed resonant structure of low energy hadrons is unimportant for the computation of OPE observables in bottom decay. It appears that the only way to test this assumption (and therefore the accuracy of the HQE) is to confront the theoretical predictions with data.

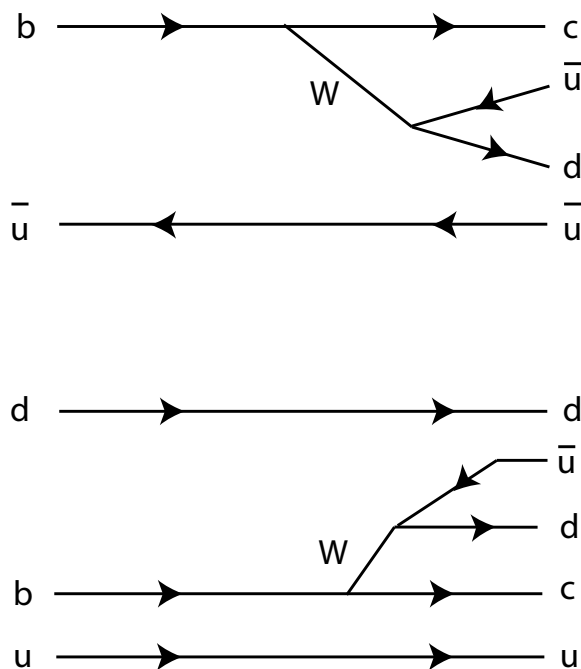


FIG. 2: Typical Pauli interference (PI) diagrams in b-hadron decay. Top: b meson decay. Bottom: b baryon decay. In general, Pauli interference includes all short-distance interactions. The diagrams demonstrate a typical contributions mediated by a charged weak boson. Pauli interference in the B^+ meson prolongs the lifetime relative to that of the B^0 , and increases the lifetime of the Λ_b by about 3%, also with respect to the B^0 .

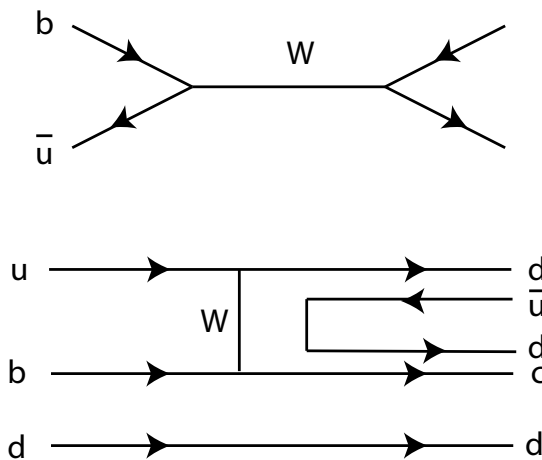


FIG. 3: Typical weak annihilation (WA) diagrams in b meson decay (top) and weak scattering diagrams in baryon decay (bottom). As in the case of PI diagrams, these are merely examples of a whole class of short distance interactions. These diagrams do not contribute much to meson lifetimes, but do decrease that of the Λ_b by about 7%.

B. Experimental Context

We present a measurement of the lifetimes of the B^+, B^0, B_s^0 and Λ_b hadrons and of the lifetime ratios τ_{B^+}/τ_{B^0} , $\tau_{B_s^0}/\tau_{B^0}$ and $\tau_{\Lambda_b}/\tau_{B^0}$. The measurement is performed using exclusive decays to states containing a J/ψ . The work reported here is based on Run II data available up to March 2006 corresponding to an integrated luminosity of 1.0 fb^{-1} . Fig. 4 illustrates the topologies of these decays.

The world average values (from PDG 2006) are presented in Table I. For the B^0 and B^+ , the world averages are dominated by a single experiment, Belle, whose published result [4] is a precombination of many channels including fully reconstructed channels with a J/ψ or with other hadrons, and semileptonic channels. Those measurements are

Lifetime (μm)		Measured Value (PDG2006)
τ_{B^+}	=	1.643 ± 0.010 ps,
τ_{B^0}	=	1.527 ± 0.008 ps,
$\tau_{B_s^0}$	=	1.454 ± 0.040 ps,
τ_{Λ_b}	=	1.288 ± 0.065 ps,
Lifetime ratio	Predicted range	Measured Value (PDG2006)
$\tau(B^+)/\tau(B^0)$	1.04 – 1.08	1.076 ± 0.008
$\bar{\tau}(B_s^0)/\tau(B^0)$	0.99 – 1.01	0.914 ± 0.030
$\tau(\Lambda_b)/\tau(B^0)$	0.86 – 0.95	0.844 ± 0.043

TABLE I: Measured values of lifetimes and lifetime ratios (from PDG2006) compared with theoretical predictions [2, 3]

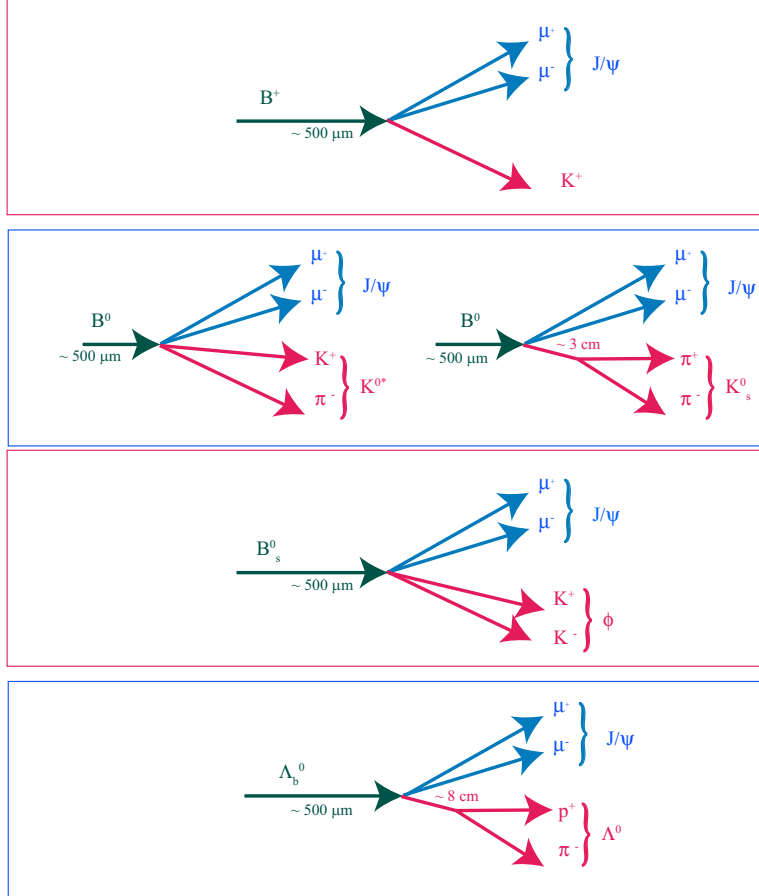


FIG. 4: Topologies of the B hadron decay channels considered.

now limited by systematic errors. As we will see, the statistical error on our B^+ lifetime is under $5 \mu\text{m}$ (0.015 ps), at approximately the 1% level. Great care is now required both to minimize and to properly estimate the systematic error of lifetime measurement. The ratio τ_+/τ_0 is also important, as it is more precisely predicted by the theory and more precisely measured in experiment, certain systematic errors cancelling in the ratio.

CDF and D0 are currently the only running experiments producing the b hadrons B_s and Λ_b , and will dominate the world average for the lifetimes of these two states. The acceptance of the D0 experiment is approximately equal to that of CDF for the decay $B_s^0 \rightarrow J/\psi \phi$, but apparently much lower than that of CDF for $\Lambda_b \rightarrow J/\psi \Lambda$: D0 reconstructs 174 events in 1fb^{-1} [5] compared to 532 in this analysis. These two lifetimes are less accurately known than those of the B^+ and B^0 , and the history of previous measurements reveals some discrepancies with theoretical expectations. A snapshot from PDG 2006 can be seen in Table I.

The goal of this set of measurements is to measure lifetimes in a consistent way across all of the five channels considered, to control systematic errors to the level necessitated by the B^0 and B^+ modes, and then to apply the same methods across the board to the other channels. We use the vertex formed by the two tracks from the J/ψ as an estimate of the transverse decay length (defined below) so that systematic errors common to the estimate of decay length cancel to some extent in the ratio of lifetimes. The resolution model is calibrated using the 7.8M inclusive J/ψ s recorded in the first 1 fb^{-1} of data. Assumptions about the universality of this resolution model within the five channels are checked finally using a special Monte Carlo simulation where the resolution model has been artificially altered by adding tails similar to those seen in the calibration sample of inclusive J/ψ events.

CDF has recently published a measurement of the Λ_b lifetime [6]. The present measurement refines the previous one by applying a new estimator of lifetime designed to correct for a systematic effect (resolution model) and further reduces the systematic error to $3.5 \mu\text{m}$. The expected magnitude of the correction is about $-5 \mu\text{m}$, as will be shown in the following sections. This is within the $5.5 \mu\text{m}$ systematic error assigned to the resolution model in [6].

The cuts are designed to minimize the statistical error on measured lifetime using Monte Carlo samples for $B^+ \rightarrow J/\psi K^+$, $B^0 \rightarrow J/\psi K^{*0}$, $B^0 \rightarrow J/\psi K_s^0$, $B_s^0 \rightarrow J/\psi \phi$ and $\Lambda_b \rightarrow J/\psi \Lambda$ signals and “far” sidebands for the background. Because we use the sidebands to determine the level and shape of the background in our lifetime fit, we define “far” sidebands which are outside of the mass region used for the fit to avoid any potential statistical bias on the lifetime (see [7] for more details). A summary of all selection cuts used to reconstruct $B^+ \rightarrow J/\psi K^+$, $B^0 \rightarrow J/\psi K^{*0}$, $B^0 \rightarrow J/\psi K_s^0$, $B_s^0 \rightarrow J/\psi \phi$ and $\Lambda_b \rightarrow J/\psi \Lambda$ is shown in Table II. The selection yields 12.9K $B^+ \rightarrow J/\psi K^+$, 4.8K $B^0 \rightarrow J/\psi K^*$, 3.6K $B^0 \rightarrow J/\psi K_s^0$, 1.1K $B_s^0 \rightarrow J/\psi \phi$, and 532 $\Lambda_b \rightarrow J/\psi \Lambda$.

The proper decay length of a b hadron is the difference (in ct) between production and decay points in the Lorentz frame of the hadron. Analysis objects used to estimate this quantity are: tracks (to estimate the b hadron four momentum and the decay point, or secondary vertex) and the beamline (to estimate the production point, or primary vertex). The transverse decay length L_{xy} of a single decay is defined as

$$L_{xy} = \frac{\mathbf{V} \cdot \vec{P}_T}{|\vec{P}_T|} \quad (2)$$

where \mathbf{V} is the vector pointing from the primary to the secondary vertex position and \vec{P}_T is the transverse momentum. Both the \mathbf{V} and \vec{P}_T are two dimensional vectors, defined in the $r\phi$ plane. The proper decay length (PDL) $c\tau$ is computed as:

$$c\tau = \frac{ML_{xy}}{P_T} \quad (3)$$

We perform an unbinned trivariate maximum log-likelihood fit to mass, PDL, and PDL error; the lifetime error in addition is used to adjust a resolution which varies on an event-per-event basis. The mass error is not a fit variable and is used only to adjust the mass resolution on an event per-event-basis. The likelihood function for invariant mass variable is written as a single Gaussian for the signal and a first-order polynomial for the background. The likelihood function for proper decay length variable is written as an exponential convolved with an event-per-event resolution function, for the signal, while for the background it is written as a combination of 1) a Gaussian, which models the prompt background, 2) two exponentials which model background from heavy flavor, and 3) a negative exponential which models other background such as pattern recognition errors, decay in flight background, etc. The prompt component is smeared by the full resolution model while the other components (described below) while the other components are smeared using a simple model with a scale factor. The likelihood for the proper decay length error variable is modelled as the sum of three gamma distributions for the signal and the sum of two gamma distributions for the background.

We incorporate the J/ψ resolution model measured in the inclusive J/ψ sample [10] (see section II A). In order to see the effect of this step, we carry out the analysis in two ways; first, we perform the fit using a simple resolution model parameterized by a proper decay time scale factor, and second, we perform a fit using a resolution model calibrated on inclusive J/ψ s. Lifetime measurements are obtained from the second fit, the first fit being merely for comparison. The use of the calibrated resolution model calibrates away many potential systematic effects (such as displacements of the beam line and certain types of misalignments), and also makes it unnecessary to consider them individually in the error analysis.

In CDF, the model of proper time resolution has till now normally been taken to be a single Gaussian described by the error estimate $\sigma_{c\tau}$ multiplied by a collective scale factor, $\sigma_{c\tau}$ having been obtained by propagation of tracking errors to vertex errors to the proper decay time with the use of formula 2 and 3.

A study of 7.8 M J/ψ events in a dedicated study [10] indicates that a three-component model for the resolution is more accurate for inclusive J/ψ 's than a simple model. Fig. 5 shows the invariant mass of events used in that study. A fit to the mass distribution is used to define signal and sideband regions; then the sideband-subtracted L_{xy} distribution is fit, using various models to describe the resolution function.

The best resolution model that could be found for the data has two Gaussian components which scale with the estimated error, and a third Gaussian component unrelated to the estimated error. The parameters of the model are: fractions for each component, scale factors for the first two components, and width for the third. The inclusive $J/\psi L_{xy}$ distribution (before resolution smearing) is modeled as a prompt component plus a positive exponential from B decays, whose fraction floats. Parameters of the model are then adjusted to fit the sideband-subtracted L_{xy} distribution. This procedure is carried out within six bins of $\Delta\phi$, the opening angle between J/ψ daughter tracks. Since material in the hybrid boards is concentrated at the ends of detectors in the silicon system, the events are also classified as to whether they lie in the ‘‘hybrid region’’ where multiple scattering effects are larger, or in the ‘‘silicon region’’ where they are smaller. Parameters of the model are presented in [10].

Fig 6 shows the residuals from several of these fits, compared with the residuals from the simple, single-Gaussian model. The superiority of the the three-component model can be clearly seen from these plots. It clearly cannot be reasonably maintained that a simple, single Gaussian description of resolution is correct for lifetime measurement.

Toy Monte Carlo can be used to estimate the shift in lifetime when the simple model is used to estimate data distributed according to the three-component model. In estimating these shifts, toy Monte Carlo was generated according to the three-component model described above, and fit with the simple model with floating scale factor. The parameters governing the resolution model are taken from [10]. This model is parameterized differently within bins of the z -coordinate of the vertex position of the J/ψ and within bins of opening angle. Opening angles and z vertex positions are distributed according to the data. Two variants of the three component model are used: one which incorporates a small shift in the resolution model, another which centers all three components on $c\tau = 0.0$.

The average value taken from the distribution of shifts is tabulated in Table III. This table shows that the use of a simplified resolution model affects lifetime measurement by shifting, the measured lifetimes by 4-5 μm , for all channels considered in this note. Both signal and background were generated in this study.

B. Results

We apply the resolution model described above (for signal and prompt background) in the lifetime fits to the five decay channels considered in this analysis. The lifetime measurements performed with this resolution model, summarized in Table IV, differ from those extracted using the simple model in two ways:

- The extracted lifetimes shift downward, as expected, by amounts between 0 and 4 μm .
- Generally speaking the objective function ($-2\ln\mathcal{L}$) is lower when the calibrated resolution model is used[12]

This later point is quite interesting, since the resolution model used to obtain B hadron lifetimes in not adjusted at all to the B data, but instead to the calibration sample of 7.8 M J/ψ events. The full set of parameters used in the fit are described in the Table VI. The fitted quantities appear in Table V. Likelihood projections in the mass, PDL, and PDL error variables are shown in Figs 7, 8, 9, 10, 11. In Fig 12, 13 and 14 we show the residual and residual significance distributions using the single-component model, and the three component models for the signal and sidebands regions for the relevant modes with higher statistics. There is a significant improvement when using the three component model. We take the lifetimes extracted from this fit as nominal.

C. Systematics and cross checks

Many systematic effects enter the lifetime analysis via the resolution function. By calibrating the resolution model, we remove such effects, or rather, we absorb them into the resolution model. Two sources of error were considered for the resolution model. The first, called the modeling error, accounts for the fact that the residual plots in Fig 6 still do not indicate a perfect fit. To account for this we used Toy Monte Carlo to evaluate the shift between the shifted and the unshifted model. It was found to be negligible. The second error related to the resolution function comes from

the assumption that the resolution model measured using inclusive J/ψ events applies to J/ψ from B decays: since a χ^2 cut on the b -hadron vertex is applied, the selection procedure can affect the resolution. Before checking this with full simulation, we increased the tails in the L_{xy} pull distribution by adding additional smearing to roughly the level observed in the inclusive J/ψ data. The resolution indeed is biased, we found, by the χ^2 cut. Systematic errors arising from this effect were evaluated in to Monte Carlo. Since the observed shift varied with channel, this systematic error does not fully cancel in the ratio of lifetimes. The alignment error is evaluated by moving the detectors in and out, and bowing them in and out, by the 50 micron uncertainty estimated by the alignment group (this is not redundant with the resolution uncertainty because it changes the overall distance scale). The background model was evaluated by introducing a flat component as well as a family of “glitch” functions near the origin generated by Hermite Polynomials times a Gaussian envelope (one obtains in this manner normalized functions *not* constructed by adding Gaussians). The mass model was varied by allowing a second Gaussian in the peak, and by allowing a quadratic term in the mass model for the background. In the case of the B^+ , a component describing the mass distribution of the Cabibbo suppressed $B^+ \rightarrow J/\psi K^+$ was also added. To evaluate the error from the modeling of the PDL error, we tried an alternate model of PDL error which was also found to fit the data: the sum of two smeared exponentials with a common displacement from zero. All errors were evaluated using Toy Monte Carlo, except for the alignment error which was evaluated using full simulation.

In the past CDF has worried about the effect of V^0 pointing in the $B^0 \rightarrow J/\psi K_s^0$ and $\Lambda_b \rightarrow J/\psi \Lambda$ modes. The effect is supposed to influence lifetime measurement by introducing a PDL-dependent selection bias, rather than by influencing the determination of $c\tau$. In this analysis we find this error to be negligible. To determine this we looked at the pointing of “neutral tracks”. A sample of inclusive K_s^0 was selected. Small distortions in the d_0/σ_{d_0} distribution were seen. We amplified these by a factor of ≈ 20 (up to $\pm 1 \sigma$), and re-introduced them into full simulation by displacing the daughter tracks. The marginal effect of the additional smearing is to reject an additional 1% of events. The lifetime distribution of the additional events is consistent with that of the full sample. So we argue that the mechanism cannot affect measured lifetimes. The results of the systematics are summarized in Table VII.

As a final check the calibration of the resolution model, we applied free scale factors in the following three ways:

- A free scale factor is added to the signal PDF.
- A free scale factor is added to the prompt background PDF.
- A free scale factor is added to both the signal PDF and the prompt background PDF.

The scale factors are applied on top of the calibrated resolution function.

The results are shown in Table. VIII. None of the minimum $-2 \ln \mathcal{L}$ values has changed by more than four units. When we apply the scale factor to only the signal, it’s determination is as expected very poor, only about 10% of its value. When the scale factor is applied to the background, the determination is less than 1%, and then the value we extract is less than but very close to unity. Lifetime values change by very little. We assign no systematic as the probable cause of the deviation from unity (the effect of the χ^2 cut) has already been investigated and separately quantified. This gives us additional confidence in our resolution model.

III. SUMMARY

We have measured the lifetimes of exclusive decays of B^+ and B^0 mesons to a J/ψ and a kaon, B_s^0 meson to a J/ψ and a ϕ and Λ_b baryon to a J/ψ and a Λ . The results are shown below. The central values and statistical uncertainties are taken from the values for simultaneous mass-lifetime-PDL_error fit listed in table V, and the systematic uncertainties are taken from table VII.

$$\begin{aligned}
c\tau(B^+ \rightarrow J/\psi K^+) &= 488.6 \pm 4.8(stat) \pm 3.2(syst)\mu m \\
c\tau(B^0 \rightarrow J/\psi K^{*0}) &= 471.3 \pm 7.6(stat) \pm 3.7(syst)\mu m \\
c\tau(B^0 \rightarrow J/\psi K_s^0) &= 457.1 \pm 8.8(stat) \pm 3.2(syst)\mu m \\
c\tau(B_s^0 \rightarrow J/\psi \phi) &= 447.9 \pm 16.2(stat) \pm 2.8(syst)\mu m \\
c\tau(\Lambda_b \rightarrow J/\psi \Lambda) &= 473.8 \pm 23.1(stat) \pm 3.5(syst)\mu m
\end{aligned}$$

We combine the two B^0 measurements into a single lifetime measurement performing its weighted mean. The result is:

$$c\tau_{B^0} = 465.1 \pm 5.8(stat) \pm 3.2(syst)\mu m \tag{4}$$

The correspondent value for the lifetimes in picoseconds is :

$$\begin{aligned}
\tau_{B^+} &= 1.630 \pm 0.016(stat) \pm 0.011(syst)ps \\
\tau_{B^0} &= 1.551 \pm 0.019(stat) \pm 0.011(syst)ps \\
\tau_{B_s^0} &= 1.494 \pm 0.054(stat) \pm 0.009(syst)ps \\
\tau_{\Lambda_b} &= 1.580 \pm 0.077(stat) \pm 0.012(syst)ps
\end{aligned}$$

Finally, we calculate the ratio of lifetimes.

$$\begin{aligned}
\tau_{B^+}/\tau_{B^0} &= 1.051 \pm 0.023(stat) \pm 0.004(syst) \\
\tau_{\Lambda_b}/\tau_{B^0} &= 1.018 \pm 0.062(stat) \pm 0.007(syst)
\end{aligned}$$

and also

$$\tau_{B_s^0}/\tau_{B^0} = 0.963 \pm 0.047(stat) \pm 0.005(syst) \tag{5}$$

Where the latter result is to be understood as an average lifetime of B_s^0 decaying into $J/\psi \phi$. Comparison with other experiments and with PDG2006 average values are show in Fig.(17, 18, 19, 20, 21).

Acknowledgments

We thank the Fermilab staff and the technical staffs of the participating institutions for their vital contributions. This work was supported by the U.S. Department of Energy and National Science Foundation; the Italian Istituto Nazionale di Fisica Nucleare; the Ministry of Education, Culture, Sports, Science and Technology of Japan; the Natural Sciences and Engineering Research Council of Canada; the National Science Council of the Republic of China; the Swiss National Science Foundation; the A.P. Sloan Foundation; the Bundesministerium fuer Bildung und Forschung, Germany; the Korean Science and Engineering Foundation and the Korean Research Foundation; the Particle Physics and Astronomy Research Council and the Royal Society, UK; the Russian Foundation for Basic Research; the Comision Interministerial de Ciencia y Tecnologia, Spain; and in part by the European Community's Human Potential Programme under contract HPRN-CT-20002, Probe for New Physics.

-
- [1] F. Gabbiani, *et. al.*, "The Λ_b lifetime puzzle in heavy-quark expansion", hep-ph/0303235.
 - [2] C Tarantino Eur. Phys. J. **C33**, S895 (2004), hep-ph/0310241; F. Gabbiani, A. Onishchenko, and A. Petrov Phys. Rev. D68, 114006, 2003.
 - [3] F. Gabbiani, A. Onischenko and A. Petrov, Phys. Rev. **D70** 094031
 - [4] K. Abe *et. al.* (Belle Collaboration) , Phys. Rev. **D71** 072003 (2005)
 - [5] The D0 Collaboration, D0 Note 5179-Conf
 - [6] A. Abulencia *et. al.*, (CDF Collaboration) hep-ex/0609021
 - [7] Elliot Lipeles, Mark Neubauer, Frank Wuerthwein, "Measurement of Λ_b lifetime in Λ_b to $J/\psi \Lambda$ ", CDF note 7503.
 - [8] G. Punzi, "Comments on Likelihood fits with variable resolution", PHYSTAT2003, SLAC Sep. 8-11, 2003; <http://arxiv.org/abs/physics/0401045>.
 - [9] "Estimating the Size of the Punzi Effect on Lifetime Measurements in the $B^0 \rightarrow J/\psi K_s^0$ Channel," J. Boudreau it et al., CDF note 7782
 - [10] K. Anikeev *et al.*, "Studies of the proper time resolution using the J/psi sample", CDF note 8215.
 - [11] The predicted ranges in this table are from a review by the Heavy Flavor Averaging Group. Some people believe however that the lower bound on the Λ_b lifetime obtains from unnatural assumptions introduced partially in order to accomodate lower experimental values, and that the true "natural" value of $\tau(\Lambda_B)$ is closer to 0.94 (I. Bigi, private communication).
 - [12] However the B^+ does not appear to "like" the shifted resolution model.

	Cut Quantity	Value		
Muon Tracks	N($r - \phi$) SVX hits	≥ 3		
	$p_T(\mu)(\text{GeV})$	≥ 1.5		
Non-Muon Tracks	N(COT-axial)*	≥ 2		
	N(COT-stereo)*	≥ 2		
Muons	Muon Type	CMU,CMP,CMUP,CMX (type ≤ 7)		
	χ_x^2 for CMU, CMX	≤ 9		
J/ψ	mass (GeV)	$3.104 \leq m(\mu\mu) \leq 3.174$		
	2 track fit $P(\chi^2)$	> 0.001		
	Cut Quantity	$B^+ \rightarrow J/\psi K^+$	$B^0 \rightarrow J/\psi K^{*0}$	$B_s^0 \rightarrow J/\psi \phi$
K^+, K^{*0}, ϕ	$L_{xy}(\text{cm})$	-	-	-
	2 track fit $P(\chi^2)$	-	> 0.001	> 0.001
	mass(GeV)	-	$0.84 \leq m(K\pi) \leq 1.14$	$1.008 \leq m(KK) \leq 1.032$
	$p_T(\text{GeV})$	≥ 2.0	≥ 3.0	≥ 2.5
	$L_{xy}/\sigma_{L_{xy}}$	-	-	-
	Λ/K_s^0 veto (GeV)	-	-	-
	4 track fit $P(\chi^2)$	> 0.001	> 0.001	> 0.001
B^+, B^0, B_s^0	$p_T(\text{GeV})$	≥ 6.2	≥ 6.4	≥ 5.0
	Cut Quantity	$B^0 \rightarrow J/\psi K_s^0$	$\Lambda_b^0 \rightarrow J/\psi \Lambda$	
K_s^0 and Λ	$L_{xy}(\text{cm})$	≥ 0.1	≥ 0.1	
	2 track fit $P(\chi^2)$	> 0.001	> 0.001	
	mass(GeV)	$0.473 \leq m(\pi\pi) \leq 0.523$	$1.107 \leq m(p\pi) \leq 1.125$	
	$p_T(\text{GeV})$	$\geq 1.$	≥ 2.6	
	$L_{xy}/\sigma_{L_{xy}}$	≥ 6.0	≥ 4.0	
	Λ/K_s^0 veto (GeV)	$1.1085 \leq m(p\pi) \leq 1.1235$	$0.482 \leq m(\pi\pi) \leq 0.511$	
B^0, Λ_b^0	4 track fit $P(\chi^2)$	> 0.0001	> 0.0001	
	$p_T(\text{GeV})$	≥ 4.0	≥ 4.0	

N(COT-axial/stereo) refers the the number of COT axial/stereo superlayers with ≥ 5 hits.

TABLE II: All cuts used in reconstruction of $B^+ \rightarrow J/\psi K^+$, $B^0 \rightarrow J/\psi K^{*0}$, $B^0 \rightarrow J/\psi K_s^0$, $B_s^0 \rightarrow J/\psi \phi$ and $\Lambda_b \rightarrow J/\psi \Lambda$.

Mode	Number of Trials	Shift (microns)	
		3-C model with shift	3-c model no shift
$J/\psi K^+$	1200	+4.83	+4.00
$J/\psi K^{*0}$	3600	+3.64	+3.77
$J/\psi K_s^0$	7200	+4.93	+4.98
$J/\psi \phi$	20000	+3.87	+3.96
$J/\psi \Lambda$	48000	+3.86	+4.89

TABLE III: The table shows the shift in estimated lifetime when a single Gaussian is used to model data distributed according to the three-component resolution model as determined in [10] . These numbers have been estimated using toy Monte Carlo (see text for details).

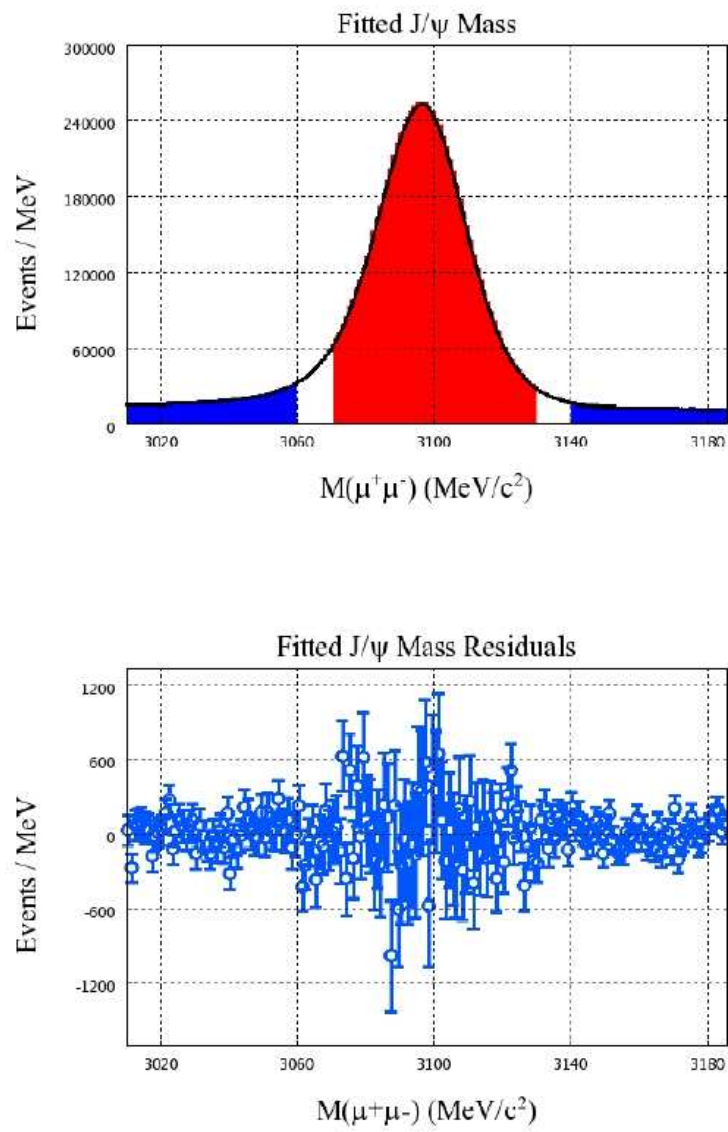


FIG. 5: J/ψ event sample used to study the resolution model: invariant mass (top) and mass residuals (bottom), i.e. data-fit from top. Error bars in the top part are not visible due to the high statistics.

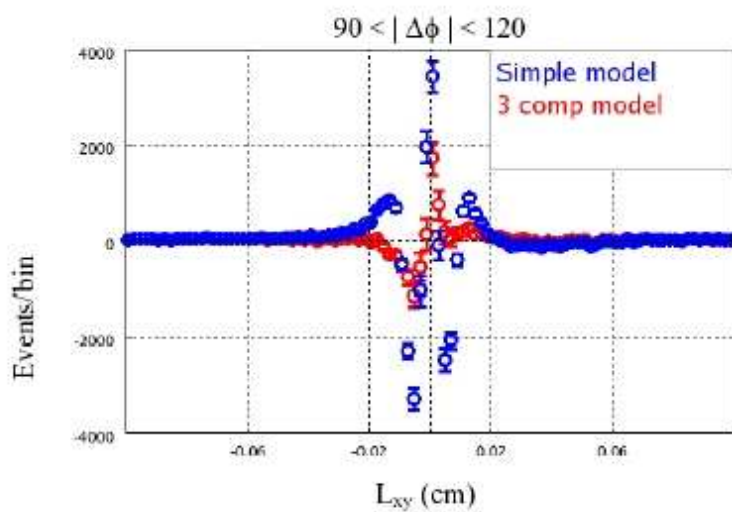
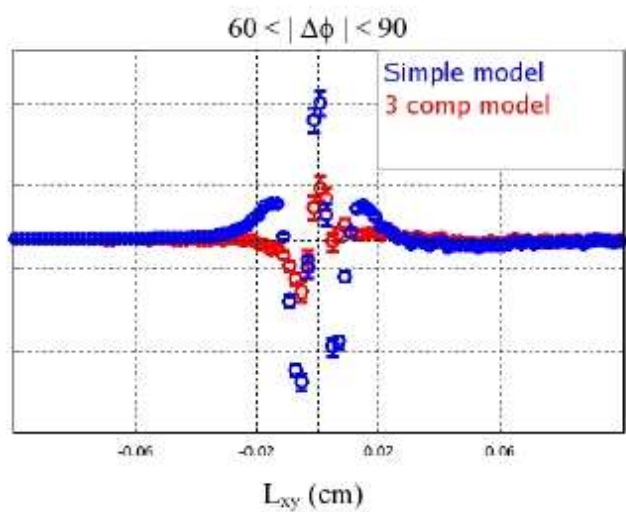
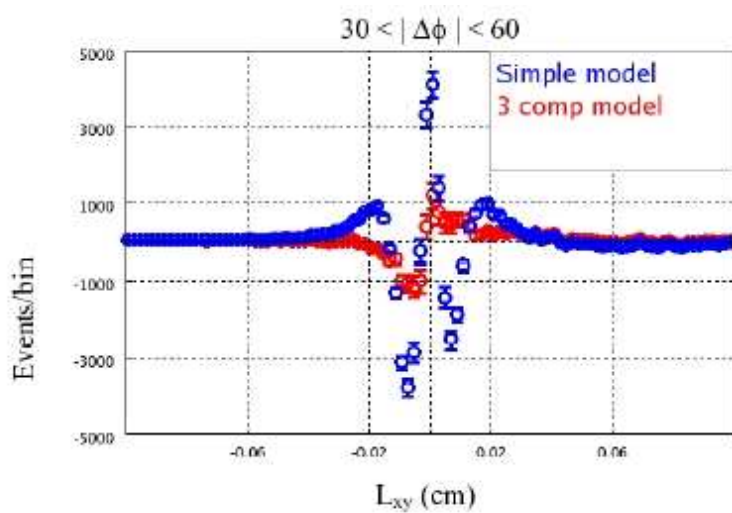
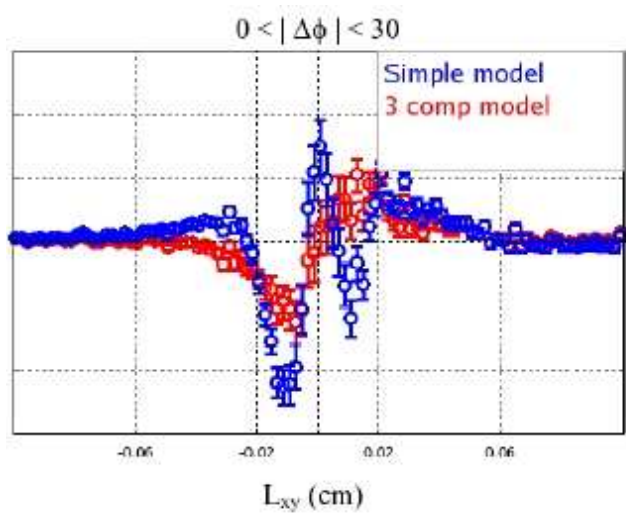


FIG. 6: Residuals from a fit to J/ψ L_{xy} data using a 3 component-model (in the silicon region) compared to residuals from a fit using the simple model (one scale factor).

	single component model $c\tau_B$ (mum)	3-component model with shift $c\tau_B$ (μm)	3-component model without shift $c\tau_B$ (μm)		
$B^+ \rightarrow J/\psi + K^+$	490.3+-4.8	488.4+-4.8	488.6+-4.8		
$B^0 \rightarrow J/\psi + K_s^0$	461.7+-8.9	458.3+-8.6	457.1+-8.8		
$B^0 \rightarrow J/\psi + K^{*0}$	472.8+-8.5	471.6+-7.6	471.3+-7.6		
$B_s \rightarrow J/\psi + \phi$	450.4+-15.7	448.4+-16.3	447.9+-16.2		
$\Lambda_b^0 \rightarrow J/\psi + \Lambda^0$	473.8+-23.9	473.7+-23.8	473.8+-23.1		
	single component model $-2 \ln \mathcal{L}$	3-component model + shift $-2 \ln \mathcal{L}$	change	3-component model (no shift) $-2 \ln \mathcal{L}$	
				change	
$B^+ \rightarrow J/\psi + K^+$	-1435516	-1435324	+192	-1436043	-527
$B^0 \rightarrow J/\psi + K_s^0$	-324692	-324970	-278	-324974	-282
$B^0 \rightarrow J/\psi + K^{*0}$	-569636	-569774	-138	-569855	-219
$B_s \rightarrow J/\psi + \phi$	-114313	-114423	-110	-114422	-109
$\Lambda_b^0 \rightarrow J/\psi + \Lambda^0$	-58669	-58739	-70	-58740	-71

TABLE IV: The table shows the extracted lifetimes and $-2 \ln \mathcal{L}$ value when extracted from data using the usual 1-component model with scale factor, and using both the shifted and unshifted 3-component models

	$B^+ \rightarrow J/\psi K^+$		$B^0 \rightarrow J/\psi K^{*0}$		$B^0 \rightarrow J/\psi K_s^0$		$B_s^0 \rightarrow J/\psi \phi$		$\Lambda_b \rightarrow J/\psi \Lambda$	
Par.	value	error	value	error	value	error	value	error	value	error
N	12286	194	4707	114	3566	96	1102	53	557	40
f_p	0.76	0.02	0.60	0.02	0.41	0.06	0.10	0.04	0.07	0.02
f_m	0.02	0.01	0.00	0.00	0.06	0.01	0.08	0.01	0.05	0.01
f_g	0.89	0.01	0.82	0.01	0.84	0.01	0.76	0.01	0.83	0.01
f_1	0.179	0.002	0.171	0.003	0.208	0.004	0.189	0.007	0.167	0.008
λ_{++}	0.0424	0.0024	0.0367	0.0014	0.0479	0.0033	0.0350	0.0037	0.0232	0.0021
λ_+	0.0057	0.0006	0.0041	0.0000	0.0095	0.0030	0.1707	0.0401	0.1400	0.0299
λ_-	0.0694	0.0179	0.0534	0.0511	0.0944	0.0152	0.1257	0.0170	0.1053	0.0263
τ_B	488.6	4.8	471.3	7.6	457.1	8.8	447.9	16.2	473.8	23.1
s_m	1.38	0.01	1.51	0.02	1.73	0.03	1.57	0.06	1.72	0.08
m	5.2785	0.0001	5.2788	0.0002	5.2805	0.0002	5.3659	0.0004	5.6200	0.0006
s_l	1.56	0.08	1.79	0.02	3.18	0.27	3.45	0.43	3.93	0.41
a_1^b	17.63	0.34	16.31	0.43	12.76	0.41	17.39	1.31	14.46	0.13
a_2^b	5.2	0.1	4.3	0.2	4.6	0.4	4.9	0.5	6.8	0.2
a_3^b	0.8	0.1	0.8	0.2	1.6	0.6	0.7	0.3	0.8	0.1
a_1^s	8.5	0.2	9.3	0.4	7.5	0.3	8.7	0.6	13.3	0.2
a_2^s	1.6	0.2	2.7	0.5	1.6	0.4	1.9	1.1	6.6	0.4
b_1^b	0.00018	0.00000	0.00017	0.00000	0.00031	0.00001	0.00018	0.00001	0.00025	0.00000
b_2^b	0.00079	0.00002	0.00088	0.00004	0.00122	0.00009	0.00080	0.00008	0.00072	0.00002
b_3^b	0.01111	0.00041	0.00982	0.00065	0.00975	0.00147	0.01025	0.00142	0.00977	0.00087
b_1^s	0.0003	0.0000	0.0003	0.0000	0.0004	0.0000	0.0003	0.0000	0.0002	0.0000
b_2^s	0.00339	0.00031	0.00165	0.00025	0.00410	0.00106	0.00307	0.00113	0.00073	0.00004
f_1^b	0.731	0.010	0.796	0.013	0.816	0.020	0.733	0.042	0.737	0.033
f_2^b	0.925	0.006	0.914	0.014	0.921	0.013	0.948	0.017	0.753	0.031
f_1^s	0.148	0.007	0.162	0.014	0.122	0.022	0.130	0.025	0.185	0.029

TABLE V: Fit results for the unshifted three component resolution model. The quantity “N” in this table is not a parameter of the final fit, but rather comes from a separate mass-only fit. Other parameters are described briefly in Table VI

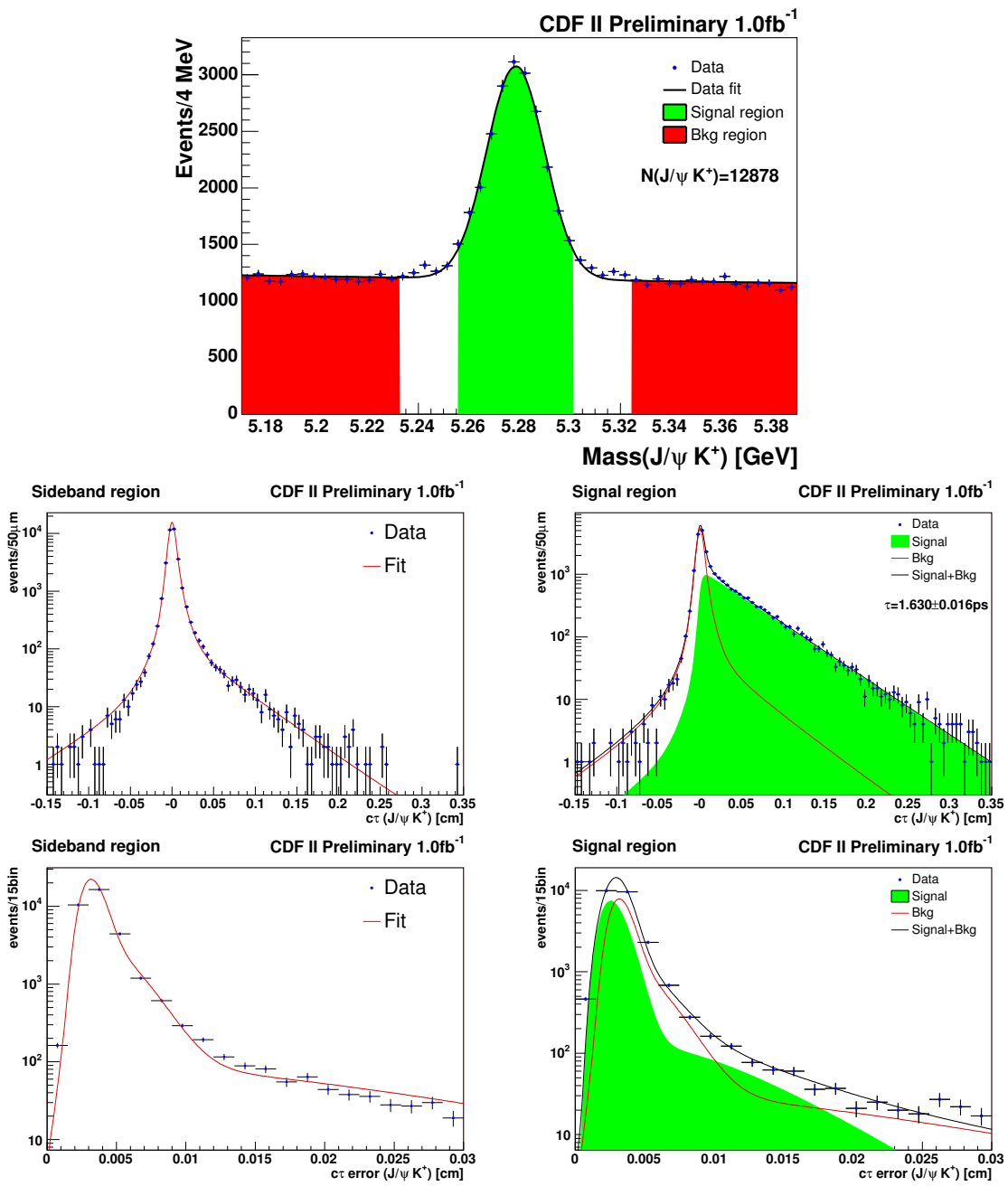


FIG. 7: $B^+ \rightarrow J/\psi K^+$. Likelihood projections in mass (top), proper decay length (PDL, middle), and proper decay length error (PDLE, bottom). Signal and sideband regions are indicated on the mass projection (top); projections of PDL and PDLE within the sideband region appear on the left, while projections within the signal region appear on the right.

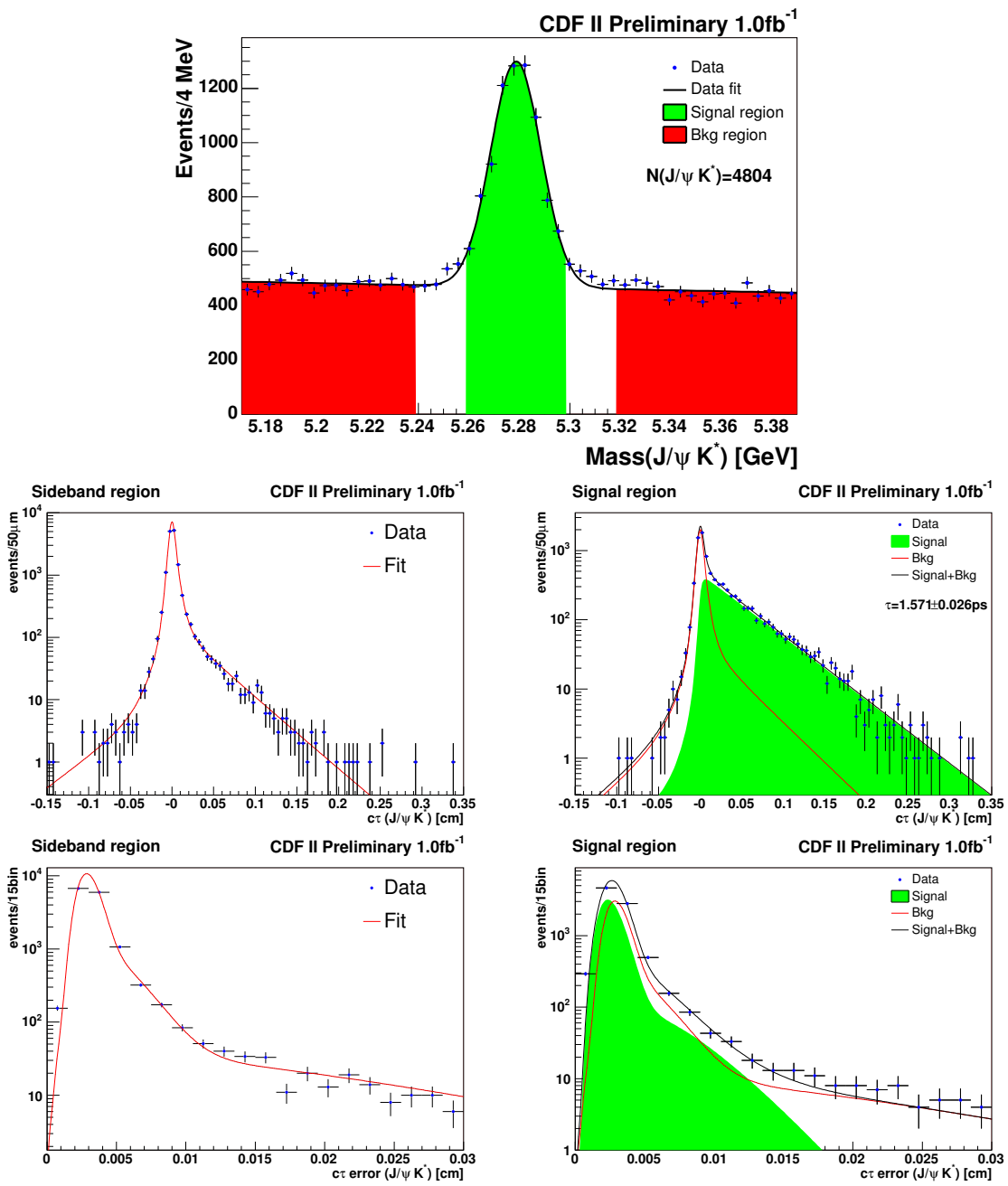


FIG. 8: $B^0 \rightarrow J/\psi K^{0*}$. Likelihood projections in mass (top), proper decay length (PDL, middle), and proper decay length error (PDLE, bottom). Signal and sideband regions are indicated on the mass projection (top); projections of PDL and PDLE within the sideband region appear on the left, while projections within the signal region appear on the right.

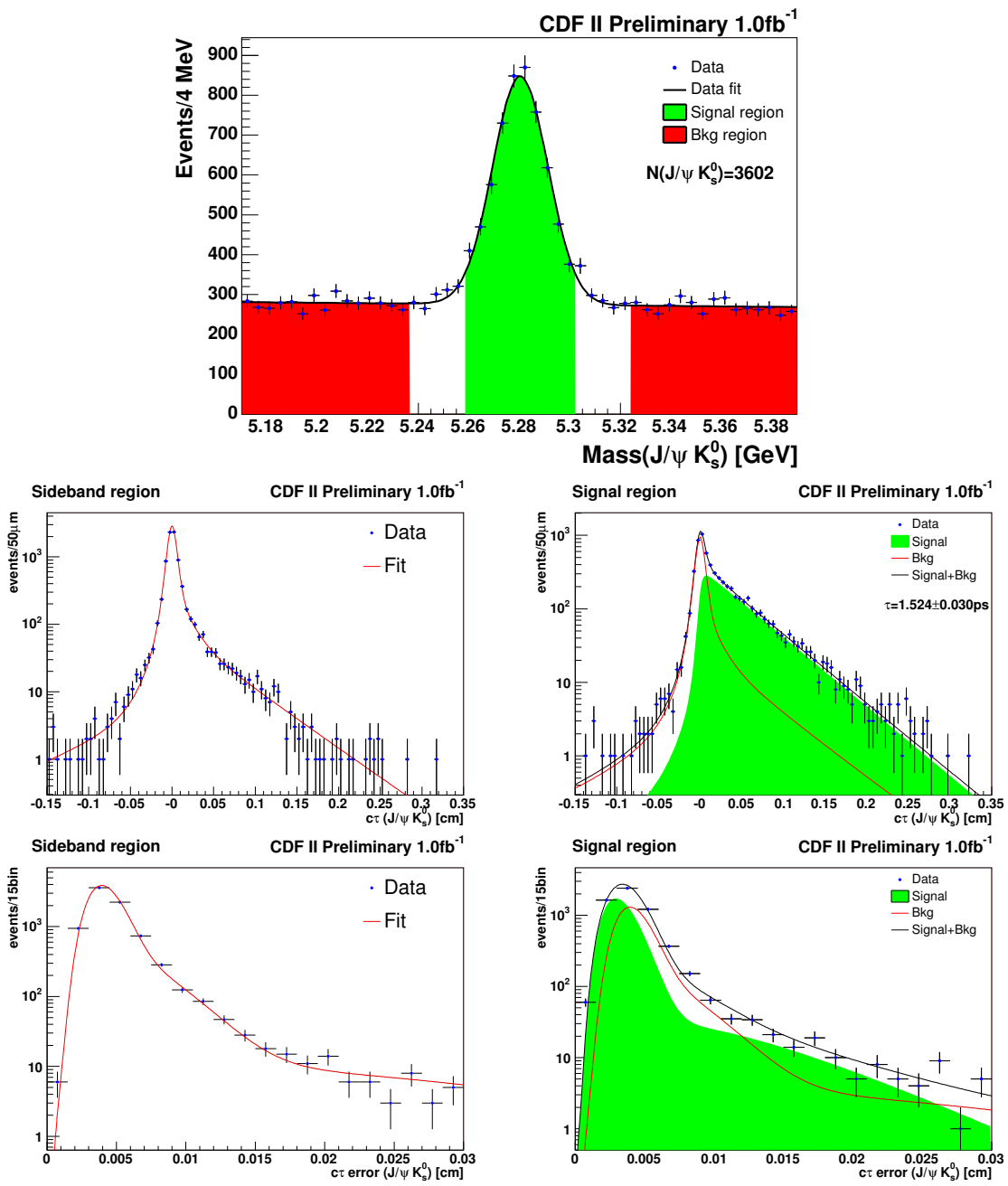


FIG. 9: $B^0 \rightarrow J/\psi K_s^0$. Likelihood projections in mass (top), proper decay length (PDL, middle), and proper decay length error (PDLE, bottom). Signal and sideband regions are indicated on the mass projection (top); projections of PDL and PDLE within the sideband region appear on the left, while projections within the signal region appear on the right.

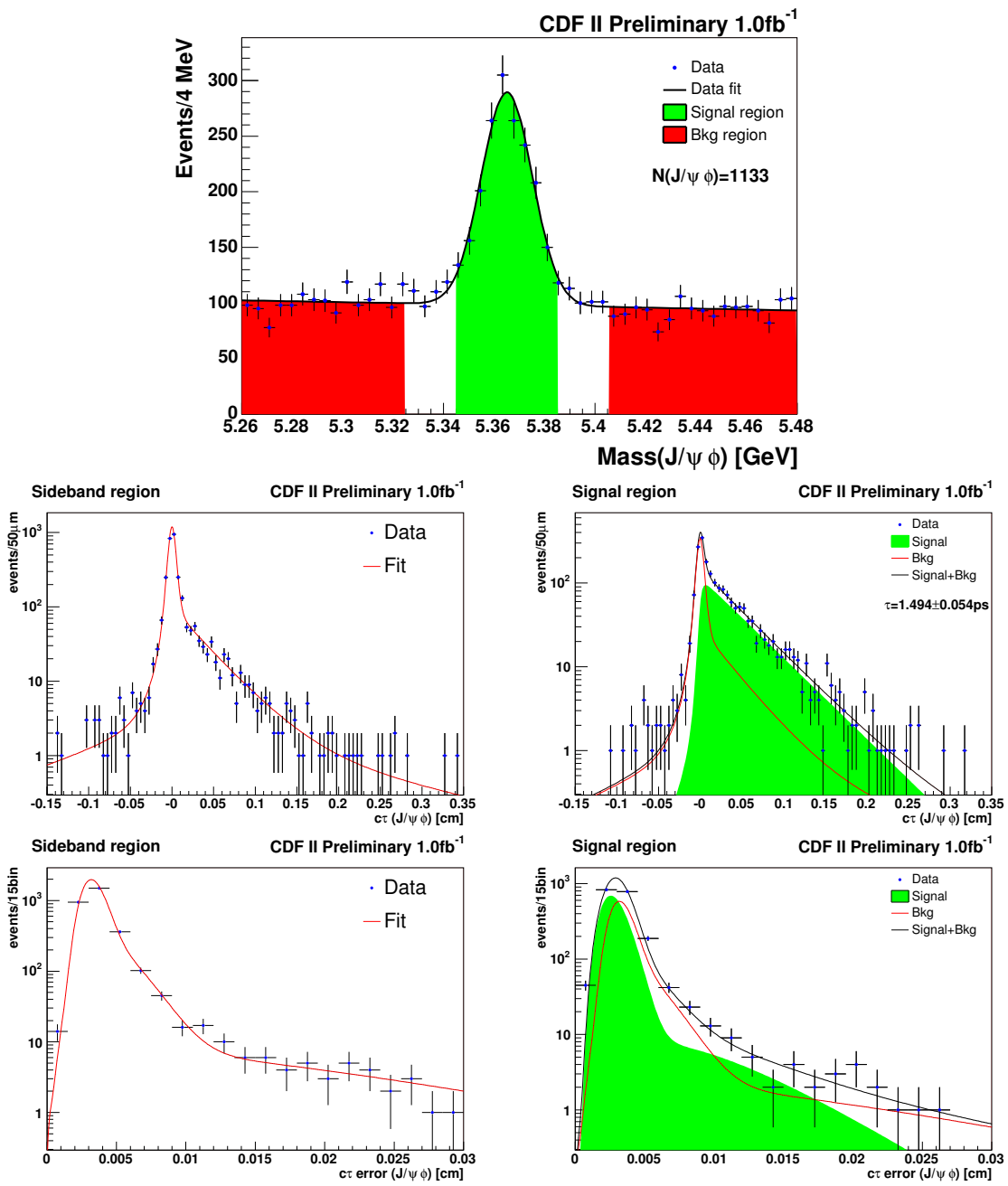


FIG. 10: $B_s^0 \rightarrow J/\psi\phi$. Likelihood projections in mass (top), proper decay length (PDL, middle), and proper decay length error (PDLE, bottom). Signal and sideband regions are indicated on the mass projection (top); projections of PDL and PDLE within the sideband region appear on the left, while projections within the signal region appear on the right.

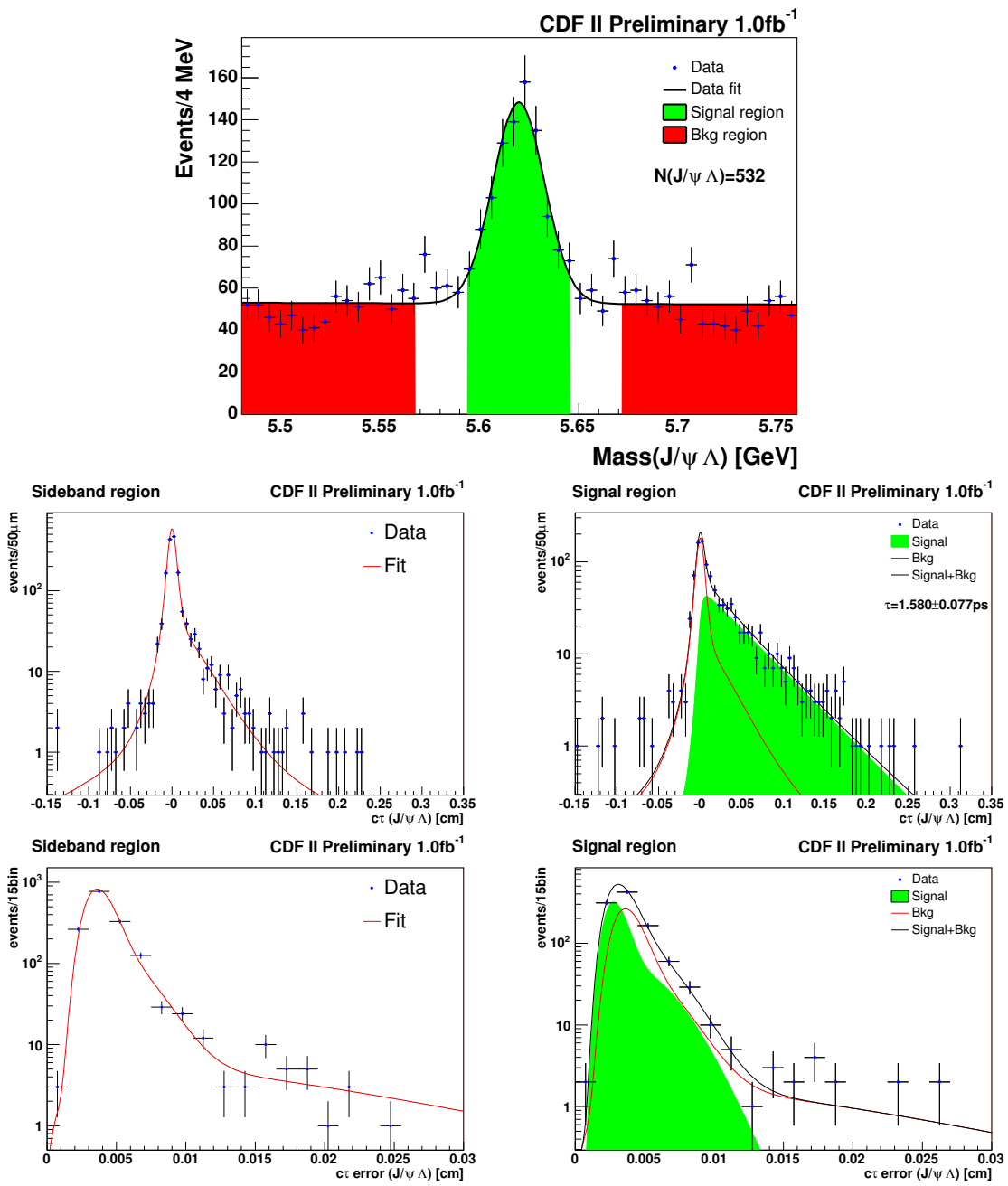


FIG. 11: $\Lambda_B \rightarrow J/\psi \Lambda$. Likelihood projections in mass (top), proper decay length (PDL, middle), and proper decay length error (PDLE, bottom). Signal and sideband regions are indicated on the mass projection (top); projections of PDL and PDLE within the sideband region appear on the left, while projections within the signal region appear on the right.

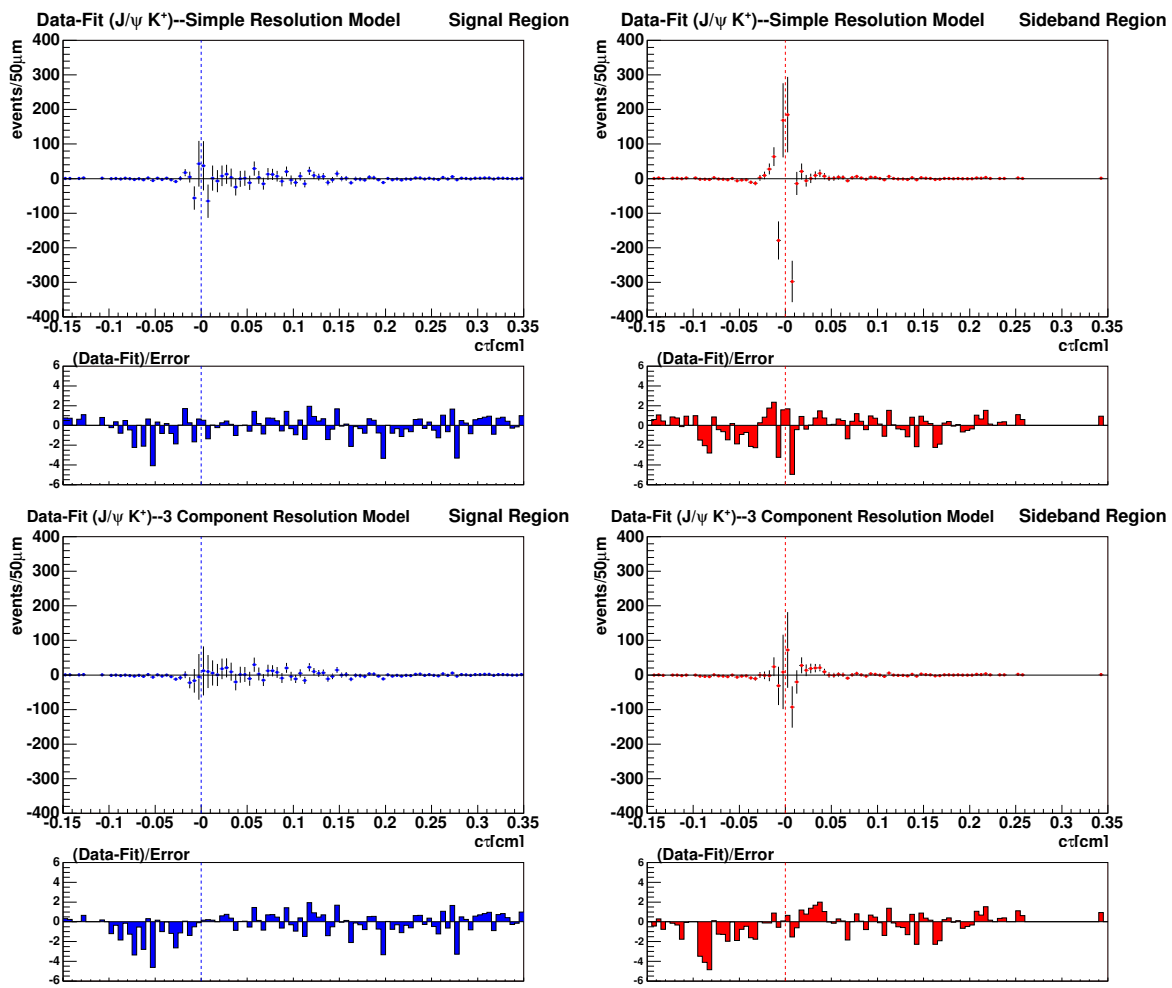


FIG. 12: Comparison of $B^+ \rightarrow J/\psi + K^+$ residual, single component resolution(top), 3-component resolution without shift(bottom). Left(right) set of plots correspond to the signal (sidebands) region respectively.

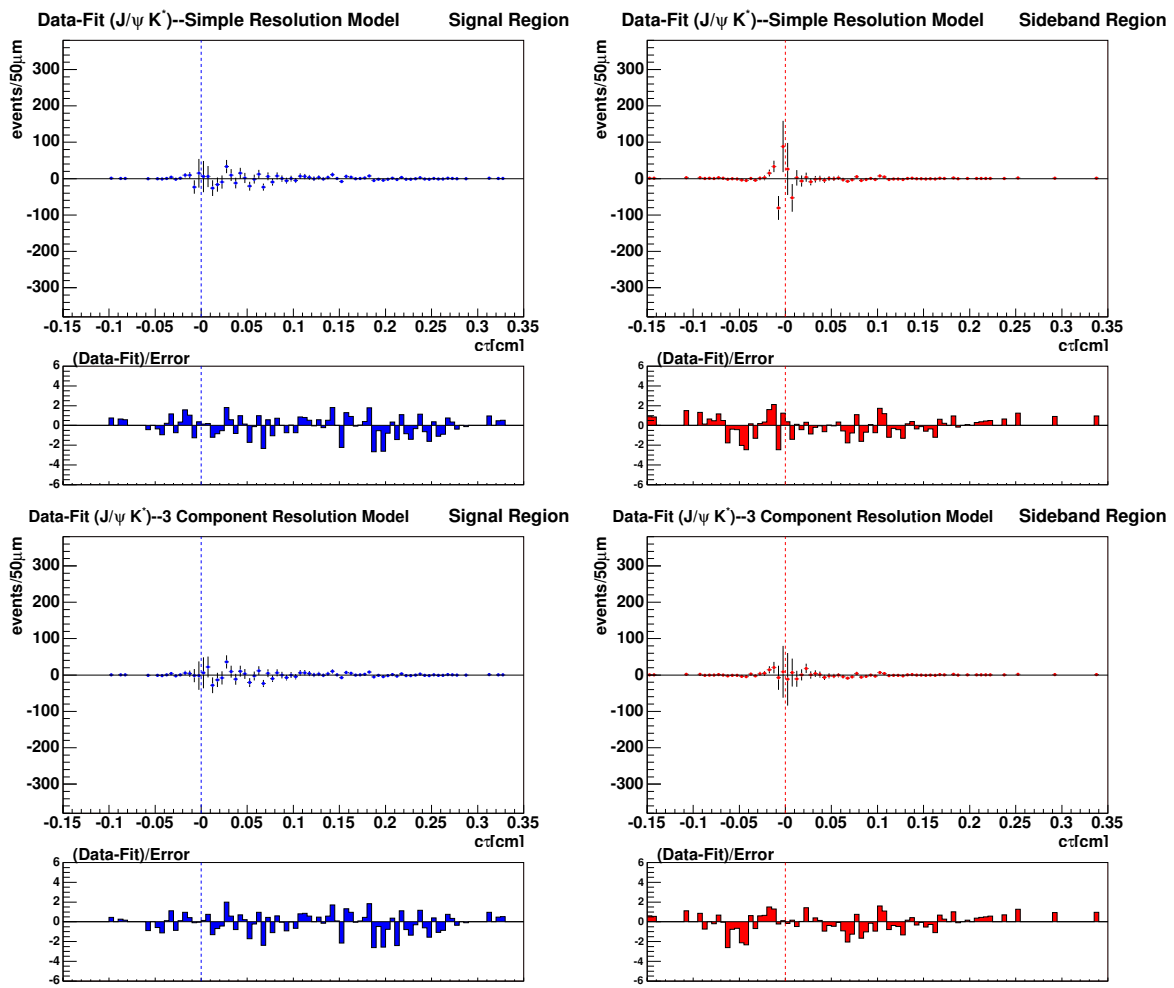


FIG. 13: Comparison of $B^0 \rightarrow J/\psi + K^{*0}$ residual, single component resolution(top), 3-component resolution without shift(bottom). Left(right) set of plots correspond to the signal (sidebands) region respectively.

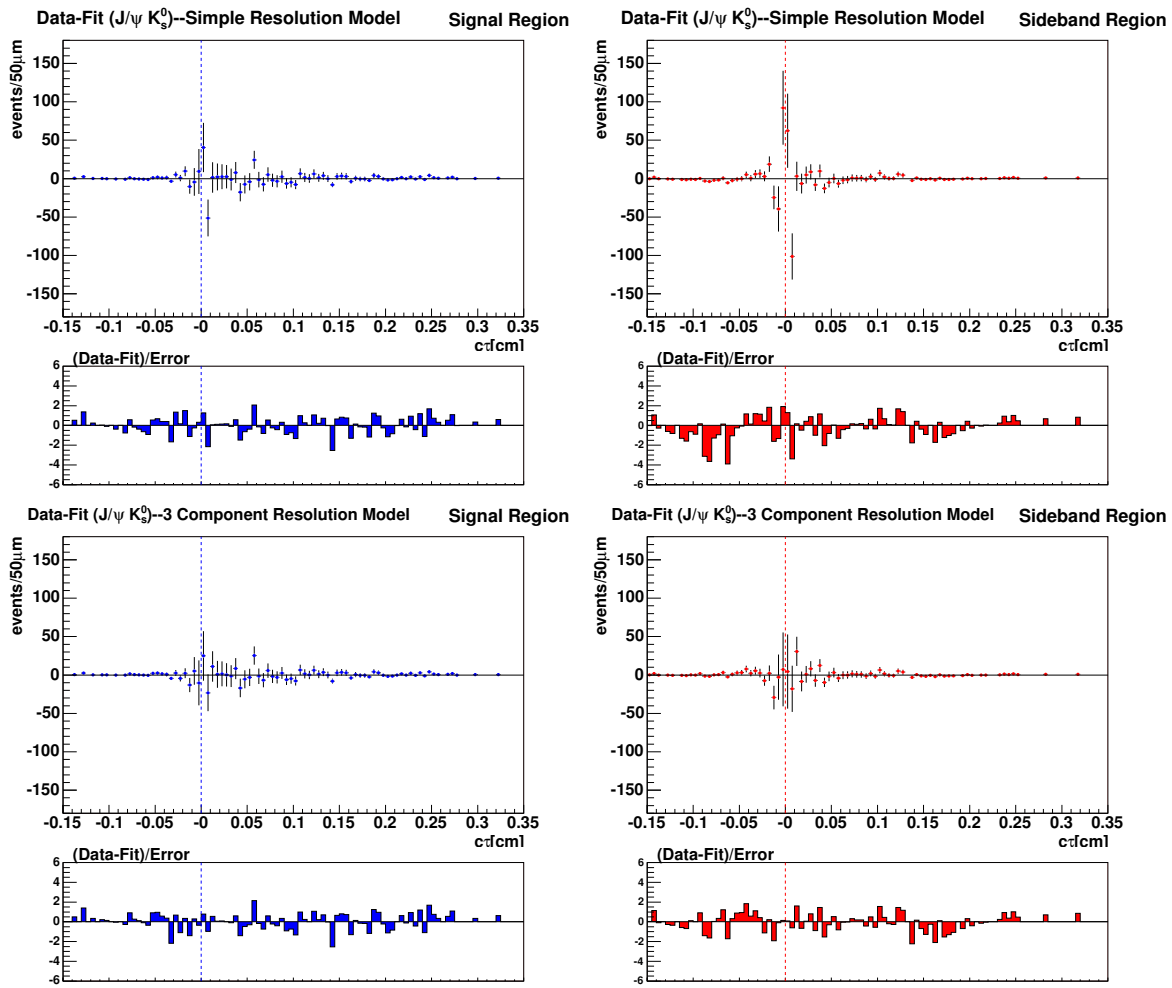


FIG. 14: Comparison of $B^0 \rightarrow J/\psi + K_s^0$ residual, single component resolution(top), 3-component resolution without shift(bottom). Left(right) set of plots correspond to the signal (sidebands) region respectively.

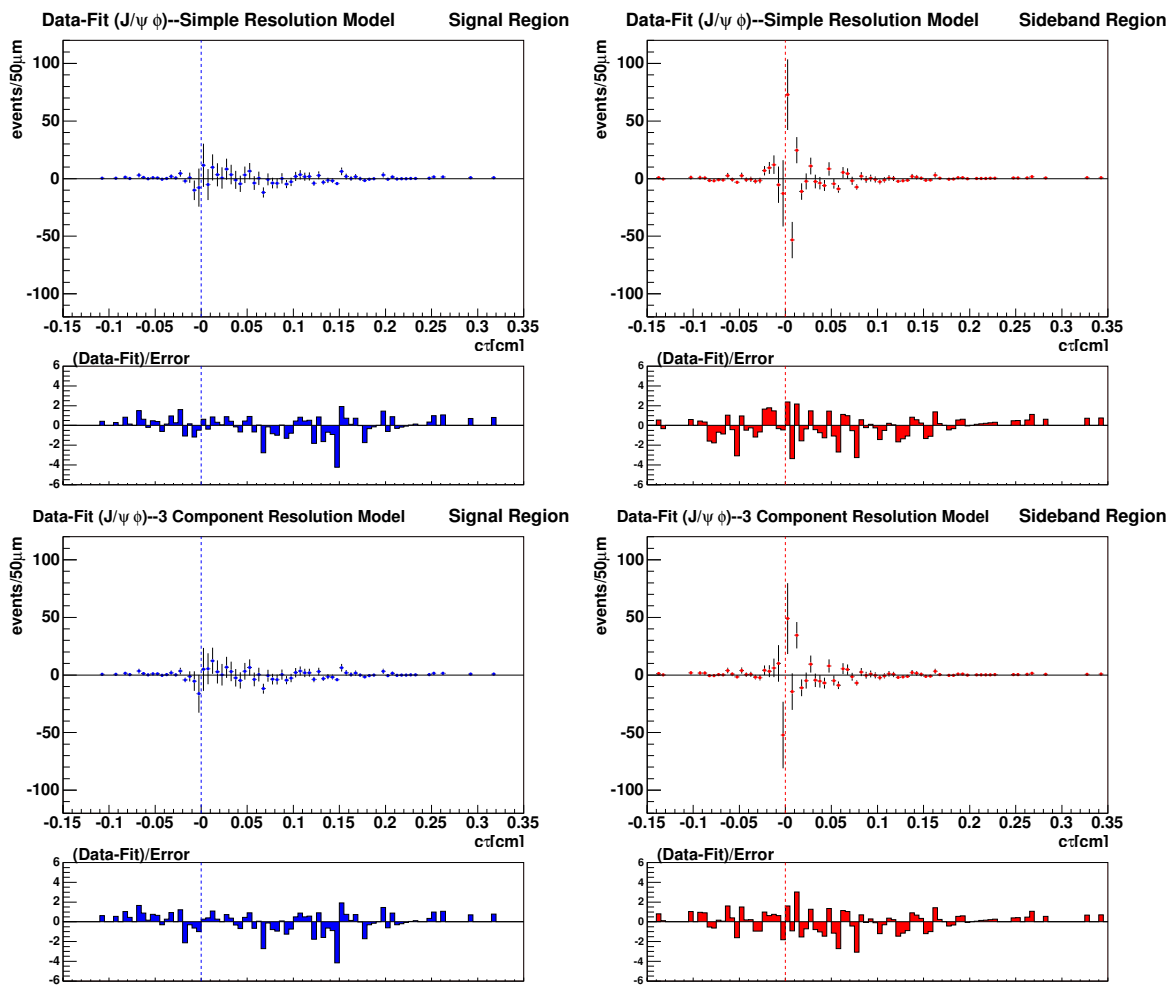


FIG. 15: Comparison of $B_s^- \rightarrow J/\psi + \phi$ residual, single component resolution(top), 3-component resolution without shift(bottom). Left(right) set of plots correspond to the signal (sidebands) region respectively.

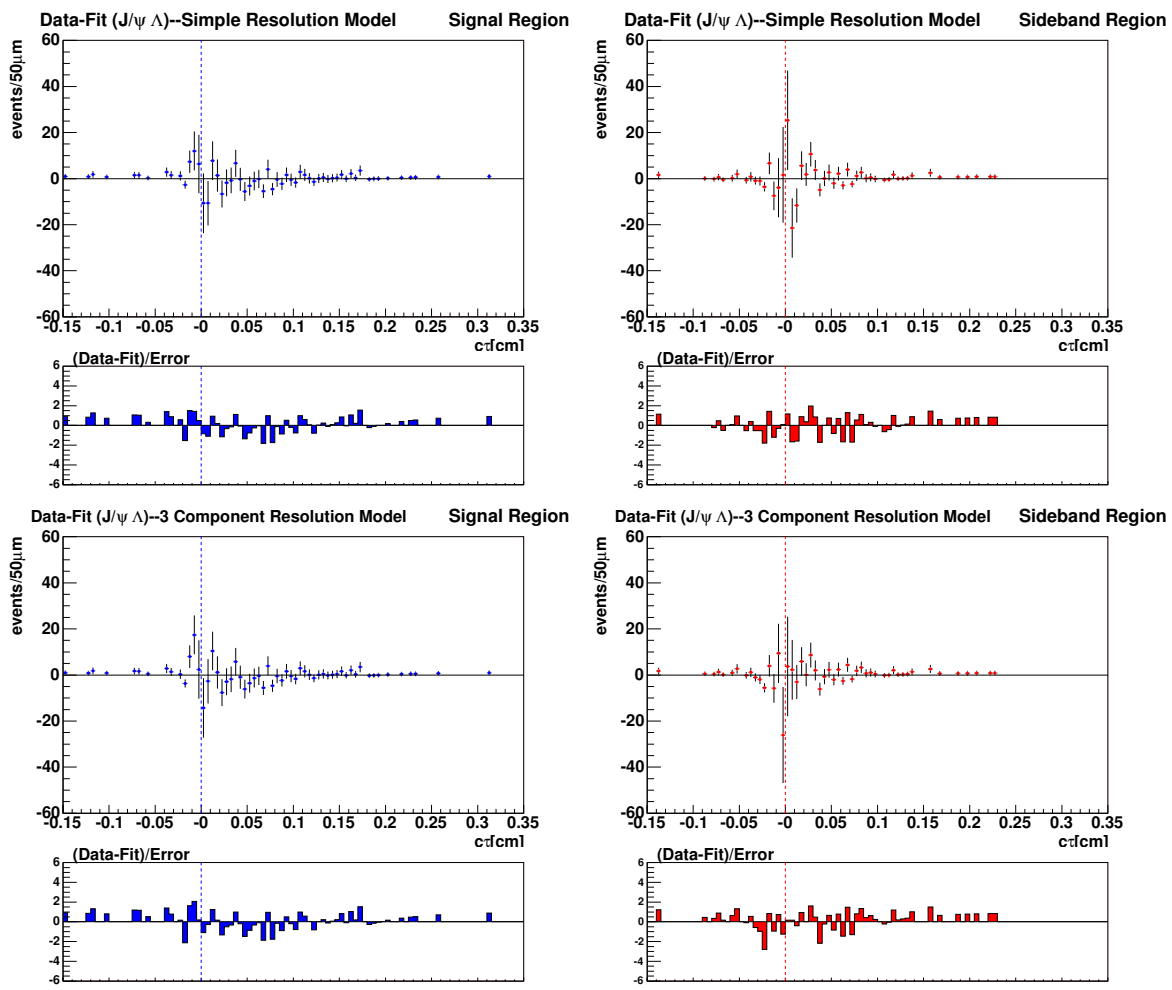


FIG. 16: Comparison of $\Lambda_b^0 \rightarrow J/\psi + \Lambda^0$ residual, single component resolution(top), 3-component resolution without shift(bottom). Left(right) set of plots correspond to the signal (sidebands) region respectively.

Name	Description	Comments
m	b hadron mass	Mass, signal
s_m	Mass Error Scale Factor	Mass, signal
P_1	Background Slope	Mass, background
s_l	Proper decay time scale factor	Proper decay time
τ_B	B hadron lifetime	Proper decay time, signal
λ_+	Effective background lifetime, pos. component 1	Proper decay time, background
λ_{++}	Effective background lifetime, pos. component 2	Proper decay time, background
λ_-	Effective background lifetime, neg. component	Proper decay time, background
f_s	Signal Fraction	Mass, Decay time, Decay time error
f_p	Fraction of remainder which is prompt	Proper decay time, background
f_{++}	Fraction of remainder which is in component 2	Proper decay time, background
f_-	Fraction of remainder which is in neg. tail	Proper decay time, background
a_1^s	a-parameter, signal, first component	PDT error, signal
b_1^s	b-parameter, signal, first component	PDT error, signal
a_2^s	a-parameter, signal, second component	PDT error, signal
b_2^s	b-parameter, signal, second component	PDT error, signal
a_1^b	a-parameter, background, first component	PDT error, background
b_1^b	b-parameter, background, first component	PDT error, background
a_2^b	a-parameter, background, second component	PDT error, background
b_2^b	b-parameter, background, second component	PDT error, background
a_3^b	a-parameter, background, third component	PDT error, background
b_3^b	b-parameter, background, third component	PDT error, background
f_1^s	fraction of signal in first component	PDT error, background
f_1^b	fraction of background in first component	PDT error, background
f_2^b	fraction of remainder (background) second component	PDT error, background

TABLE VI: Description of the full set of parameters for the unshifted three component resolution model.

Source	$J/\psi K^+$	$J/\psi K^{*0}$	$J/\psi K_s^0$	$J/\psi \phi$	$J/\psi \Lambda$	B^0
Alignment	± 2 (μm)					
Background model	+0.07 (μm)	+0.42 (μm)	-0.60 (μm)	0.72 (μm)	+0.83 (μm)	0.33 (μm)
Mass model (2^{nd} order pol. for bkg.)	-0.30 (μm)	-1.52 (μm)	-1.23 (μm)	-0.39 (μm)	-2.13 (μm)	0.99 (μm)
Mass model (2^{nd} gaussian for mass peak)	0.20 (μm)	-0.16 (μm)	-0.07 (μm)	0.03 (μm)	-0.12 (μm)	-0.07 (μm)
PDL Error	+0.59 (μm)	+0.21 (μm)	-1.31 (μm)	-0.30 (μm)	+0.33 (μm)	0.21 (μm)
Resolution universal	-2.03 (μm)	-2.36 (μm)	-1.55 (μm)	-1.13 (μm)	-1.07 (μm)	-2.1 (μm)
Resolution modelling	negligible	negligible	negligible	negligible	negligible	negligible
Cabbibo suppressed mode in B^+	-0.22 (μm)	-	-	-	-	-
V^0 pointing	negligible	negligible	negligible	negligible	negligible	negligible
Total	3.16 (μm)	3.71 (μm)	3.16 (μm)	2.77 (μm)	3.48 (μm)	3.21 (μm)

TABLE VII: Systematic Uncertainties on lifetimes in $B^+ \rightarrow J/\psi K^+$, $B^0 \rightarrow J/\psi K^{*0}$, $B^0 \rightarrow J/\psi K_s^0$, $B_s^0 \rightarrow J/\psi \phi$, $\Lambda_b \rightarrow J/\psi \Lambda$ and combined B^0 (in μm)

Mode	scale factor	$-2 \ln \mathcal{L}$	change	$c\tau$ (μm)	change
Default		-1436043		488.6 ± 4.8	
Signal Only	0.823 ± 0.099	-1436046	-3	489.7 ± 4.7	+1.1
Background Only	0.986 ± 0.004	-1436047	-4	488.9 ± 4.8	+0.3
Both	0.985 ± 0.008	-1436047	-4	488.9 ± 4.6	+0.3

TABLE VIII: The effect of free scale factors in the B^+ mode.

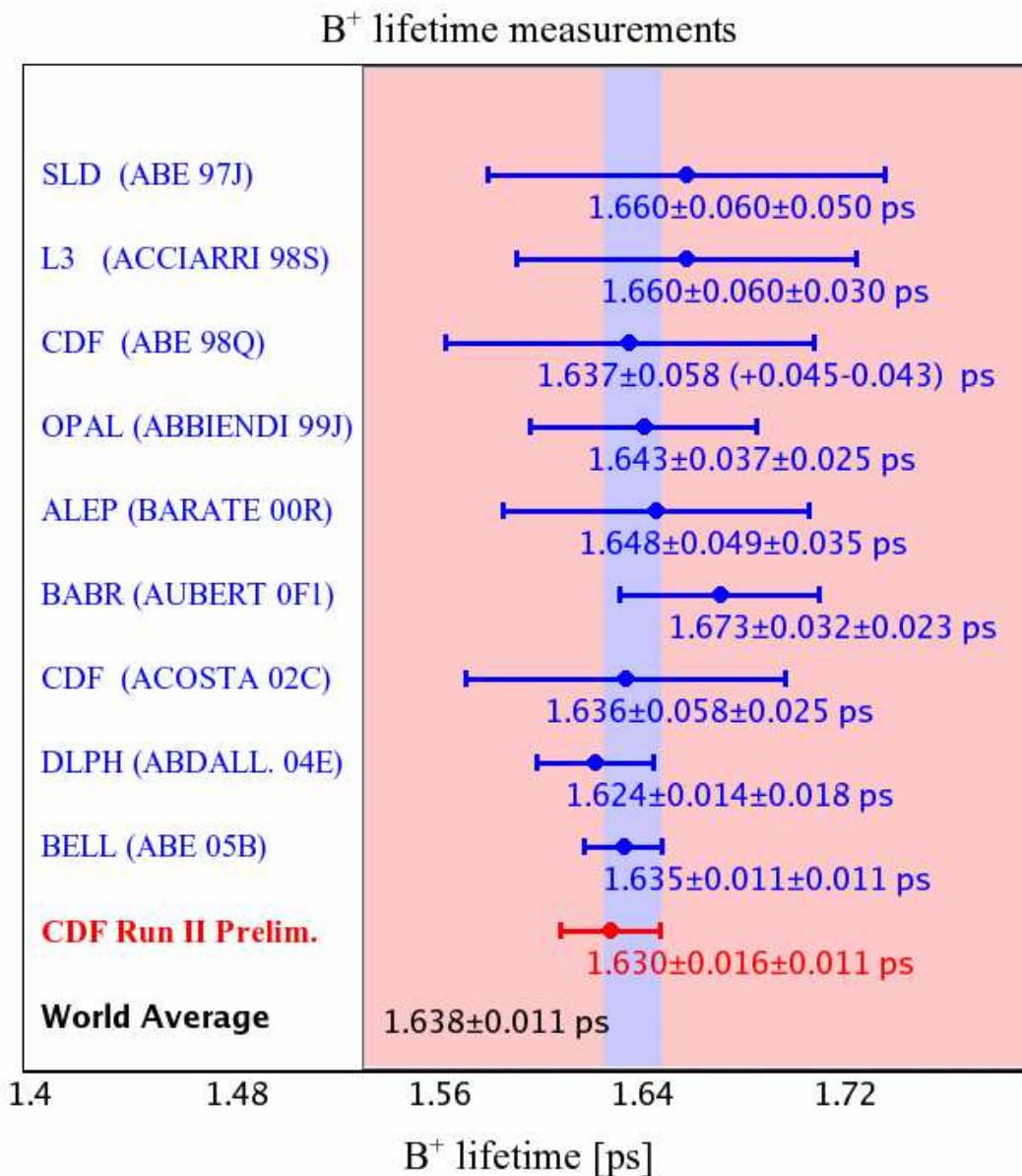


FIG. 17: Comparison of the B^+ lifetime with a selection of results quoted in the PDG2006. Note: the world average values are from PDG2006 and do not include the CDF preliminary results.

B⁰ lifetime measurements

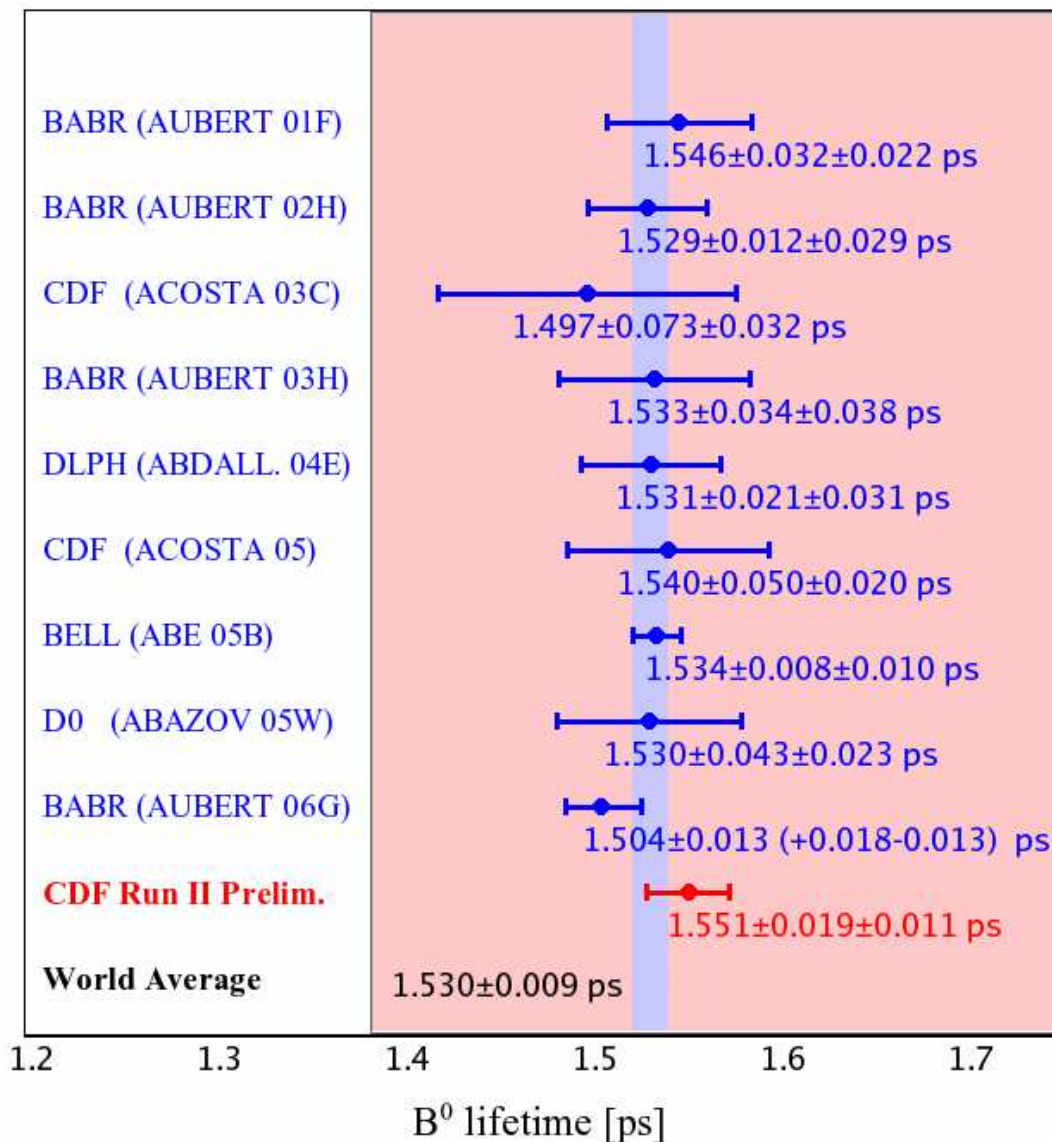


FIG. 18: Comparison of the B^0 lifetime with a selection of results quoted in the PDG2006. Note: the world average values are from PDG2006 and do not include the CDF preliminary results.

$\tau(B^+)/\tau(B^0)$ ratio measurements

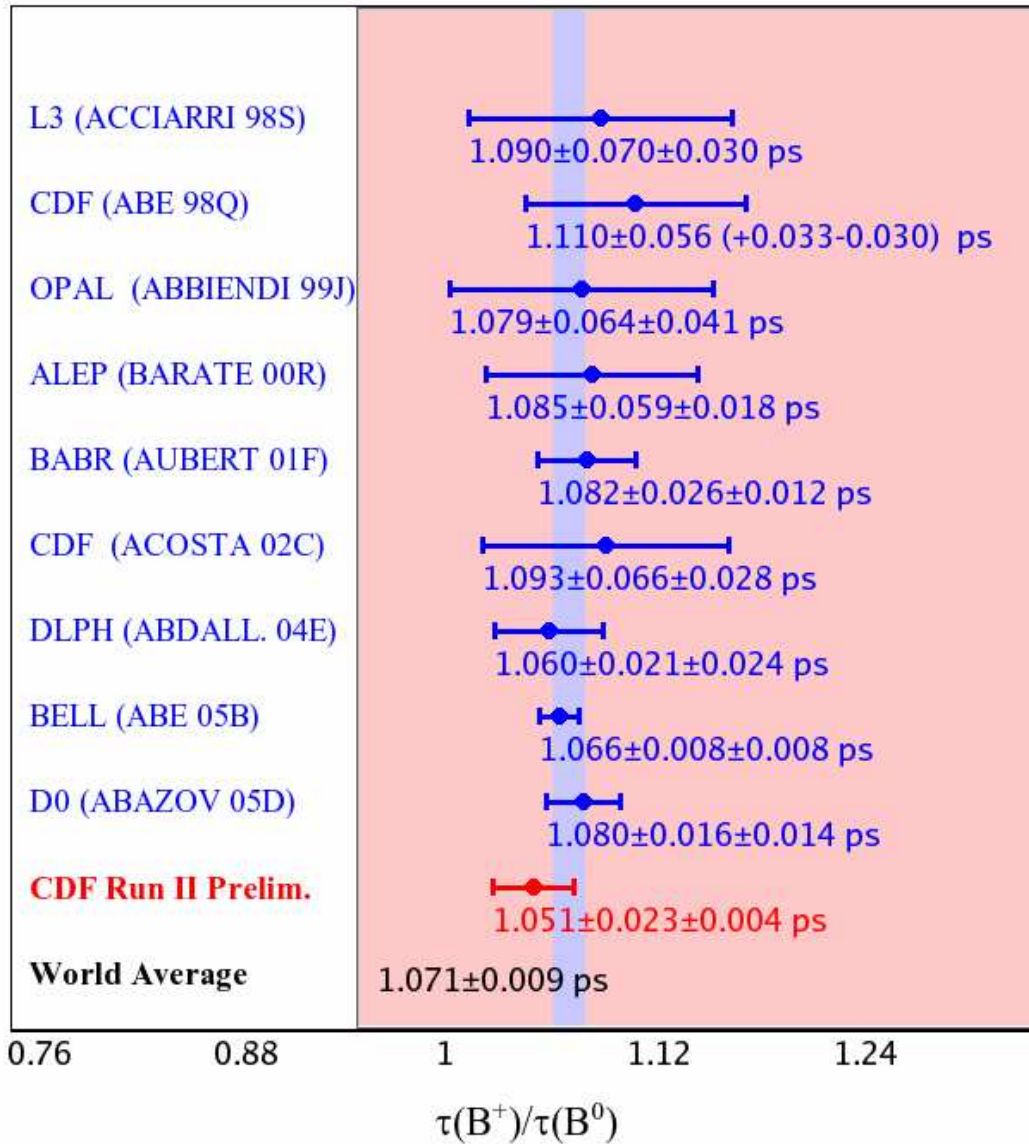


FIG. 19: Comparison of the $\tau(B^+)/\tau(B^0)$ lifetime ratio with a selection of results quoted in the PDG2006. Note: the world average values are from PDG2006 and do not include the CDF preliminary results.

$B_s^0 \rightarrow J/\psi \phi$ lifetime measurements

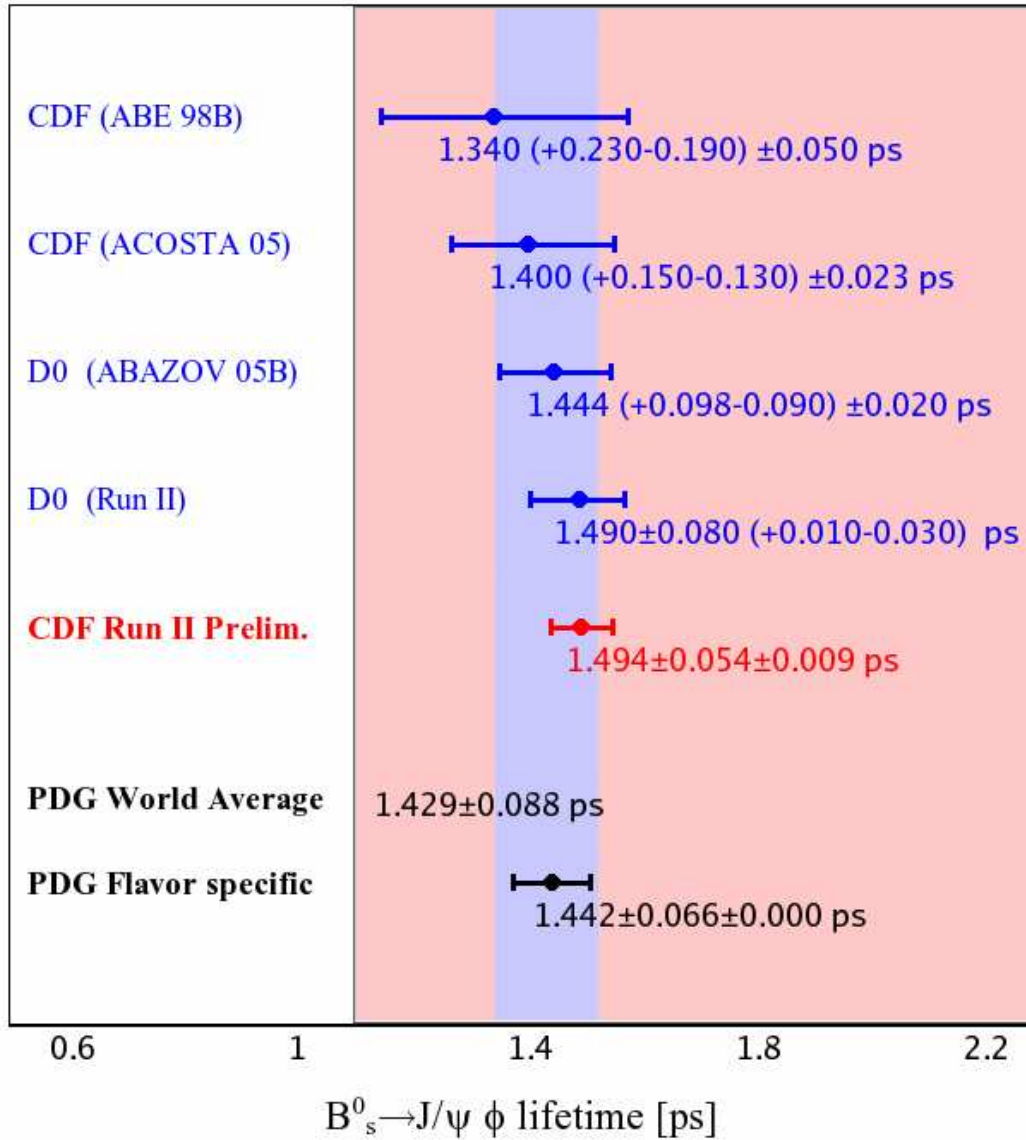


FIG. 20: Comparison of the B_s^0 lifetime with a selection of results quoted in the PDG2006 and D0's recent measurement (<http://arxiv.org/abs/hep-ex/0604046>). Note: the world average values are from PDG2006 and do not include the CDF preliminary results.

Λ_b lifetime measurements

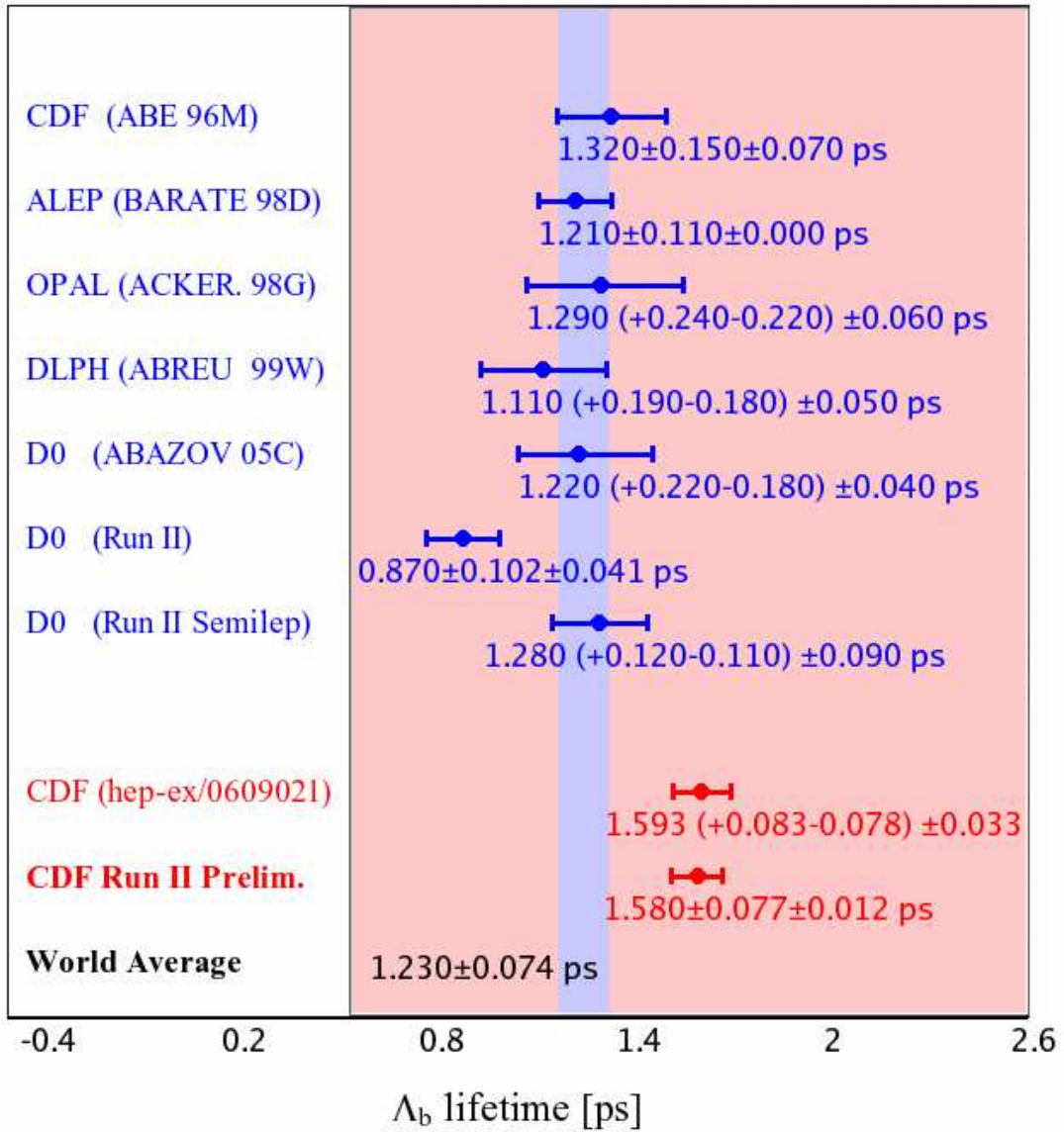


FIG. 21: Comparison of the Λ_b lifetime with a selection of results quoted in the PDG2006 and CDF's recent measurement. Note: the world average values are from PDG2006 and do not include the CDF preliminary results.